

INVESTIGATION INTO ROUGHNESS CHARACTERISTICS BY
MEASURING ANGULAR DISTRIBUTION USING He-Ne LASER

*A Thesis Submitted
in partial fulfilment of the requirements
of the Degree of*

MASTER OF TECHNOLOGY

by

RAJNISH KASHYAP

to the
LASER TECHNOLOGY PROGRAMME
INDIAN INSTITUTE OF TECHNOLOGY KANPUR

MAY, 1990

28/5/90
D

CERTIFICATE

It is certified that the work contained in the thesis entitled **Investigation into Roughness Characteristics by Measuring Angular Distribution using He-Ne Laser** by Mr Rajnish Kashyap, has been carried out under our supervision and that this work has not been submitted elsewhere for a degree.

KK Sharma

(K K Sharma)

Professor and Head
Laser Technology Programme
Indian Institute of Technology,
Kanpur 208 016

G S Kainth

(G S Kainth)

Professor
Dept of Mechanical Engineering
Indian Institute of Technology,
Kanpur 208 016

May, 1990

LTP-1990-M-KAS-DNV

15 SEP .030

CENTRAL LIBRARY

Acc. No. A.108920.

ACKNOWLEDGEMENT

I express my sincere respects and gratitude to Dr.G.S.Kainth and Dr.K.K.Sharma for their invaluable guidance,suggestions and cooperation rendered during the whole course of this investigation.

I heartly thank the CELT workshop group, Mr.Om Prakash , Mr.V.S.Yadav , Mr.V.K.Bajpai and Mr.S.D.Sharma for their unlimited help and cooperation given and specially for their 11° clock tea.The effeciency with which they have handled my jobs has always helped me to keep things on a right footing.

Many thanks to Mr.D.K.Kanaujia for his invaluable assistance rendered at times when progress seemmed difficult.I am greatful to Mr.O.P.Bajaj, Mr.J.S.Sharma. Mr.S.N.Gosian . Mr.Ahmed , and Mr.R.M.Jha for providing me with necessary equipment needed for the experimental work.

Many thanks to Mr.A.K.Khullar. Mr.B.K.Jain . Mr. Ravi Shukla and Mr.Pant for giving final touch to my thesis.A salute to the newly installed Hewlett-Packard 9000 Computer Systems without which the present format of the thesis would not have been possible.

In a friendly gesture . thanks are due to my friends , Kaushik , Shukla . Mallick , Rajiv . Ravi , Diwakar ,Patni , Saxena , Avdheesh , Raghavan . Sataiah , Manzoor , Salil , Manoj , Varun , A.C.Trivedi . and the hockey team gang . Ish , Dhruv , K.Srikant , Anupam , Paliwal . David . Verma , Sangal , Vivek for their excellent companionship.

And finally as a token of respect , I thank my father
M. M. Kashyap , my mother Mrs. U. Kashyap for their constant
encouragement, inspiration, love and affection bestowed during the
whole course of my stay here.

Kashyap. R

TABLE OF CONTENTS

Page No.

List of Figures	... vii
List of Tables	... ix
Nomenclature	... x
Abstract	... xi
 CHAPTER 1	
INTRODUCTION AND LITERATURE SURVEY	
.. 1 INTRODUCTION	... 1
.. 2 DEFINITIONS OF TERMS	... 1
.. 3 PARAMETERS	... 4
.. 4 LITERATURE SURVEY	... 7
1. 4. 1 Profiling techniques	... 7
1. 4. 2 Parametric techniques	... 9
1. 4. 3 Existing theories	... 10
 CHAPTER 2	
THEORETICAL ANALYSIS	... 14
2. 1 GENERAL SOLUTION (By. Peter Beckmann)	... 14
2. 2 GENERAL KIRCHOFF SOLUTION OF THE FIELD SCATTERED BY A PERFECTLY CONDUCTING PLANE	... 22
2. 2. 1 Application to specific periodic profiles	... 25
2. 3 OBSERVATIONS	... 30
2. 3. 1 Variation of angle of incidence	... 31
2. 3. 2 Variation of h	... 32
2. 3. 3 Theoretical AD	... 33
2. 3. 4 Separation of modes	... 38
2. 4 CONCLUSIONS	... 38
2. 5 ASSUMPTIONS	... 41
 CHAPTER 3	
EXPERIMENTAL SET-UP AND PROCEDURE	... 42
3. 1 EXPERIMENTAL SET-UP	... 45
3. 1. 1 Selection of laser	... 45
3. 1. 2 Selection of photo-detector	... 45
3. 1. 3 Detector motion	... 48
3. 1. 4 Point of incidence	... 48
3. 1. 5 Need for vertical motion	... 50
3. 1. 6 Mirror mounts	... 52
3. 1. 7 Shape of specimens	... 52
3. 1. 8 Distance of detector from specimen	... 55
3. 2 PROCEDURE	... 55
3. 2. 1 Angular distribution (AD) measurement	... 55
3. 2. 2 Measurement of specular intensity I_s	... 56

CHAPTER 4	
EXPERIMENTAL RESULTS AND DISCUSSION	... 59
4.1 ANGULAR DISTRIBUTION	... 59
4.2 SPECULAR INTENSITY	... 59
4.3 ROUGHNESS PROFILE	... 70
4.4 DISCUSSION	... 70
4.4.1 Angular distribution	... 70
4.4.2 Specular intensity	... 70
CHAPTER 5	
CONCLUSIONS	... 80
APPENDIX	... 82
REFERENCES	... 85

LIST OF FIGURES

	Page No.
FIG.1.1 FOUR ORDERS OF GEOMETRIC IRREGULARITIES	... 2
FIG.1.2 SURFACE CHARACTERISTICS	... 2
FIG.1.3 NOMINAL AND MEASURED PROFILE	... 2
FIG.1.4 DEFINITION OF CENTRE LINE OR MEAN LINE	... 6
FIG.1.5 AMPLITUDE DENSITY FUNCTION	... 6
FIG.1.6 SURFACE ROUGHNESS PRODUCED BY COMMON PRODUCTION METHODS	... 8
FIG.2.1 ANGULAR DISTRIBUTION (AD) OF LIGHT SCATTERED BY A ROUGH SURFACE	... 15
FIG.2.2 BASIC NOTATION	... 15
FIG.2.3 DERIVATION OF EQUATION NO.(3)	... 18
FIG.2.4 LOCAL SCATTERING GEOMETRY	... 18
FIG.2.5 DERIVATION OF GRATING EQUATION	... 24
FIG.2.6 DIRECTIONS OF SCATTERED MODES BY PERIODIC SURFACE	... 24
FIG.2.7 PROFILE SPECIFICATIONS	... 28
FIG.2.8 FIELD AT ANY POINT P IN FRESNEL ZONE IS SUM OF AMPLITUDES SCATTERED BY DIFFERENT WAVE PERIODS	... 28
FIG.2.9 SPECULAR INTENSITY FROM A FINE GRATING	... 32
FIG.2.10 VARIATION OF SPECULAR INTENSITY WITH ROUGHNESS HEIGHT (h)	... 34
FIG.2.11 SCATTERING BY A TRIANGULAR SURFACE	... 36
FIG.2.12 THEORETICAL AD FOR A TRIANGULAR SURFACE	... 37
FIG.2.13 THEORETICAL SEPARATION OF MODES	... 39
FIG.3.1 SCATTERED INTENSITY MEASURING INSTRUMENT	... 43-44
FIG.3.2 PHOTODIODE RESPONSIVITY CURVE	... 46
FIG.3.3 AMPLIFIER CIRCUIT	... 47
FIG.3.4 C 30808 PHOTOTRANSISTOR	... 47
FIG.3.5 X-SECTION OF DETECTOR HOUSING	... 47

FIG. 3.6	SOLID ANGLE SUBSTENDED BY DETECTOR	... 49
FIG. 3.7	SURFACE VIEWED BY DETECTOR	... 49
FIG. 3.8	EFFECT ON POSITION OF POINT OF INCIDENCE WITH CHANGE IN ANGLE OF INCIDENCE BY ROTATING THE SPECIMEN	... 51
FIG. 3.9	ALLIGNMENT OF DETECTOR AND LASER	... 54
FIG. 3.10	DETECTOR ARM	... 54
FIG. 3.11	SCHEMATIC DIAGRAM OF EXPERIMENTAL SET-UP	... 57
FIG. 3.12	DIFFRACTION PATTERN AT DIFFERENT ANGLE OF INCIDENCE	... 58
FIG. 4.1	AD MEASUREMENT FOR VARIOUS ANGLES OF INCIDENCE FOR SPECIMEN NO. FA-1	... 60
FIG. 4.2	AD MEASUREMENT FOR VARIOUS ANGLES OF INCIDENCE FOR SPECIMEN NO. FA-2	... 61
FIG. 4.3	AD MEASUREMENT FOR VARIOUS ANGLES OF INCIDENCE FOR SPECIMEN NO. FA-3	... 62-63
FIG. 4.4	AD MEASUREMENT FOR VARIOUS ANGLES OF INCIDENCE FOR SPECIMEN NO. FA-4	... 64-65
FIG. 4.5	AD MEASUREMENT FOR VARIOUS ANGLES OF INCIDENCE FOR SPECIMEN NO. MA-5	... 66
FIG. 4.6	AD MEASUREMENT FOR SPECIMEN NO. MA-6	... 67
FIG. 4.7	VARIATION OF SPECULAR INTENSITY WITH INCIDENCE ANGLE	... 68-69
FIG. 4.8	SURFACE PROFILE BY TALYSURF-10 ROUGHNESS MEASURING INSTRUMENT	... 71
FIG. 4.9	PROFILE DUE TO FINITE TOOL RADIUS	... 73
FIG. 4.10	$\text{sinc}^2(x)$ AND $J_0^2(x)$... 75
FIG. 4.11	VARIATION OF SPECULAR INTENSITY WITH ROUGHNESS R_a	... 75-77
FIG. 4.12	VARIATION OF INTENSITY RATIO I_s/I_{15} WITH ROUGHNESS R_a	... 78

LIST OF TABLES

	Page No.	
TABLE 1.1	SUMMARY OF OPTICAL TECHNIQUES FOR SURFACE ROUGHNESS MEASUREMENT	...11
TABLE 2.1	MODE SPECIFICATIONS	...40
TABLE 3.1	DETECTOR SPECIFICATIONS	...46
TABLE 3.2	SPECIFICATION OF SPECIMENS	...53
TABLE 4.1	ANGLE OF RISE θ_{ir}	...74

NOMENCLATURE

AD	Angular Distribution
α	Change in Angle of Incidence (Ch.3)
I_s	Specular Intensity
k	Propagation Vector = $2\pi/\lambda$
λ	Wavelength of He-Ne Laser = 6328.193 \AA^0
Λ	Spatial Wavelength of Roughness
R	Reflection Coefficient
R_a	Roughness Average
Ratio	Λ/λ
ρ	Amplitude Scattering Coefficient
R_{15}	Ratio of Specular Intensity to Intensity in 15^0
	Off-Specular Direction
rss	Rough Surface Specimen
R_N	Nose Radius of the Tool
θ_i, θ_1	Angle of Incidence w.r.t Normal
θ_s	Scattering Angle w.r.t θ_i
θ_2	Scattering Angle w.r.t Normal
	.

Name : Kashyap , R.
Roll No. : 8811606
Programme : M.Tech./Laser Technology
Thesis Title : Investigation Into Roughness Characteristics by Measuring Angular Distribution Using He-Ne Laser.
Thesis Supervisor : Dr.G.S.Kainth and Dr.K.K.Sharma

ABSTRACT

Almost all the modern machining processes involve removal of material from a surface to give it desired shape and size. The resulting removal process creates a profile on the surface which is the cause of roughness of the surface .

A rough surface scatters a collimated beam of laser light according to the laws of physical optics. The intensity and pattern of scattered light depends upon roughness height, spatial wavelength of roughness , wavelength of incident light and angle of incidence. Lasers , because of their monochromaticity , directionality and high power density , offer a potential tool for the measurement of surface roughness. Measurement of surface roughness using lasers come under the heading of parametric technique,which involves measuring a parameter that represents some property of surface topography averaged over the illuminated area.

In the present work effort has been done to measure surface roughness of highly periodic aluminium surface by using He-Ne laser. The scattered light is assumed to be a diffraction

pattern obtained by a periodic diffraction grating of constant amplitude and wavelength . The resulting diffraction pattern consists of fine diffraction spots. The separation of diffraction spots depends upon spatial wavelength of roughness and intensity depends upon the roughness heights.

Angular distribution (ADD) of scattered light is measured for various angle of incidence for face turned and face milled aluminium specimens by an instrument designed and fabricated in CELT workshop.

Angular distribution for all specimens show a No. of peaks. However, the experimental spacing is much higher than the theoretical spacing. Therefore, it is not possible to relate peak spacing to spatial wavelength of roughness.

Variation of specular intensity I_s show that all surfaces tend to reflect most of the incident light specularly at near grazing angle of incidence. The variation of I_s with roughness shows that I_s decreases with roughness. The decrease is much steeper for $\theta_i = 85^\circ$ than for $\theta_i = 87.5^\circ$. Approximate logarithmic expression has been calculated which shows that I_s can be used for measuring R_a ranging from 0.3μ to 1.0μ at near grazing angle of incidence of 85° .

CHAPTER 1

INTRODUCTION AND LITERATURE SURVEY

1.1 INTRODUCTION

Almost all the modern machining processes involve removal of material from a surface to give it desired shape and size. The resulting material removal process creates a profile on the surface, the shape of profile being characterized by particular cutting process and cutting conditions. The generated profile may be considered as a form of 3-dimensional geometric irregularity from the intended perfectly smooth surface. The order of irregularity determines the amount of roughness of a surface. The following four orders of geometrical irregularities are recognised in standards (Fig.1.1) [1].

I-order : Arising out of inaccuracies in machine tool, deformation of a work under the cutting forces or the weight of material itself.

II-order : Caused by vibrations of machine or workpiece.

III-order : Caused by machining itself and characteristic of the process.

IV-order : Arising from rupture of material during chip removal.

1.2 DEFINITIONS OF TERMS

The following are the definitions of terms used for the study of roughness of a surface. The *surface* of an object is the boundary which separates that object from another object, substance or space. The *nominal surface* is the intended surface contour

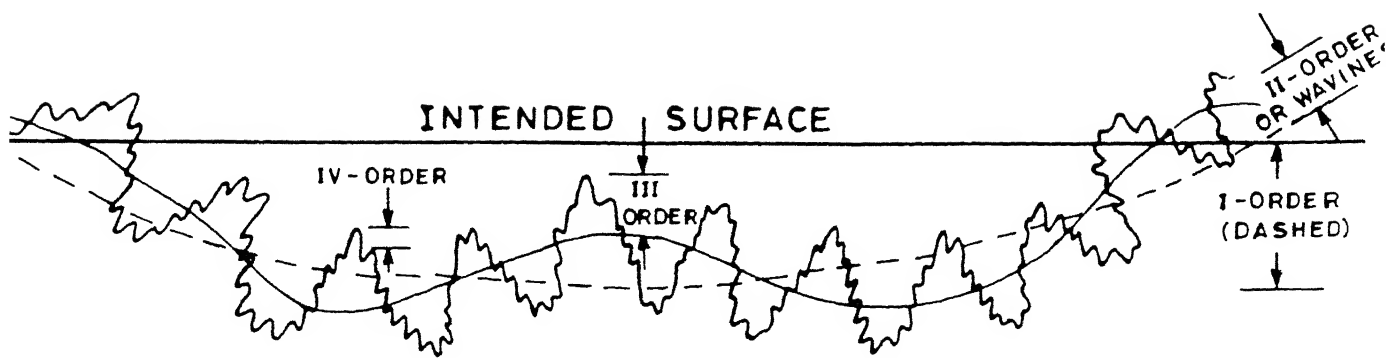


FIG. 1.1 FOUR ORDERS OF GEOMETRIC IRREGULARITIES.

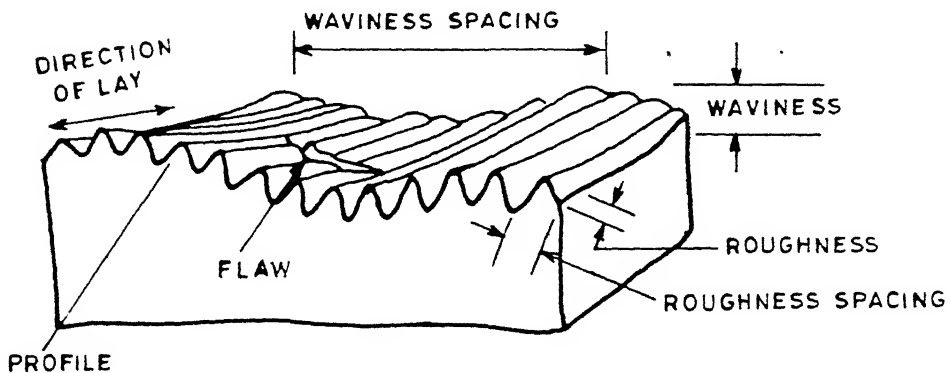


FIG. 1.2 SURFACE CHARACTERISTICS.

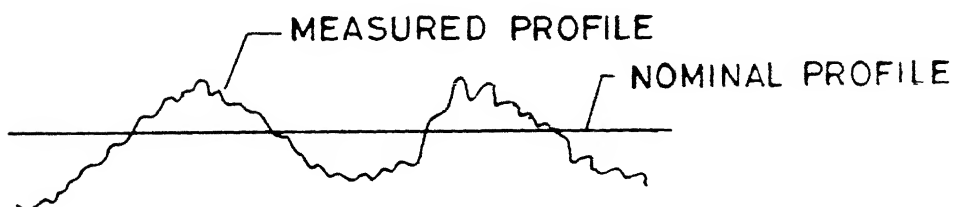


FIG. 1.3 NOMINAL AND MEASURED PROFILE.

(excluding any surface roughness), the shape and extent of which is usually shown and dimensioned on a drawing or descriptive specification. Surface texture is the repetitive or random deviations from the nominal surface which forms the three dimensional topography of the surface. Surface texture includes roughness, waviness, lay and flaws (Fig.1.2). Roughness consists of finer irregularities of surface texture which are inherent in production processes. Waviness is the more widely spaced component of surface texture upon which roughness is superimposed. Lay is the direction of predominant surface pattern, ordinarily determined by the production method. Flaws are unintentional, unexpected and unwanted interruptions in the topography. The profile is the contour of the surface in a plane perpendicular to the surface, unless some other angle is specified. The nominal profile is a profile of the nominal surface. It is the intended profile exclusive of any roughness. The measured profile is a representation of the profile obtained by instrumental or other means (Fig.1.3). The graphical centreline or the meanline (Fig.1.4-b) is the line about which roughness is measured and is a line parallel to the general direction of profile within the limits of sampling length L, such that the sum of areas embraced by the surface profile above the line are equal to sum of those below it. That is,

$$\sum (A_1 + A_3 + A_5 + \dots) = \sum (A_2 + A_4 + A_6 + \dots)$$

A peak is the point of maximum height on that portion of a profile that lies above the centreline and between two interactions of the profile with the centreline and a valley is the point of maximum depth on the portion of the profile which lies below the

centreline and between two interactions of profile with centreline (Fig.1.4-b).

1.3 PARAMETERS

Engineering surfaces are produced by a wide variety of processes resulting in variation of profile. A milled surface, for example, has a strong lay pattern, whereas, a bead blasted surface is isotropic (i.e. roughness measured along any direction is constant) and its structure is highly random. Most engineering surfaces, however, have a certain degree of anisotropy and combination of both periodic and random features. To quantify surface roughness a number of statistical functions and parameters have been developed. These characterize two basic aspects of topography, the height of asperities (amplitude) and longitudinal spacing between the asperities (spatial wavelength). For simplicity the definitions are expressed in terms of two dimensional surface profile $Z(x)$. However there are equivalent three dimensional expressions also. Assuming that profile at a crossection AA' (Fig. 1.4-a) be some curve defined by $Z = f(x)$, then:

ROUGHNESS AVERAGE R_a (also known as centreline average (CLA) or arithmetic average (AA)) represents the average deviation of surface profile about its centreline, defined as

$$R_a = \frac{h_1 + h_2 + h_3 + \dots + h_n}{L} = \frac{1}{L} \int_0^L |f(x)| dx$$

where x = distance along the surface

$f(x)$ = height of surface profile about the centreline

L = sampling length = beam dia. of laser at sample

RMS ROUGHNESS R_q (also known as σ in optics and statistics) is defined by

$$R_q = \left(\frac{1}{L} \int_0^L [f(x)]^2 dx \right)^{1/2}$$

where R_q = standard deviation of profile about the meanline. R_q is always greater than or equal to R_a .

AMPLITUDE DENSITY FUNCTION (ADF) is the probability density distribution of surface heights. It is found by plotting the histogram (Fig.1.5) of the profile points in vertical direction. If the surface is produced by truly random process, the ADF would be a Gaussian distribution of surface heights, given by:

$$ADF(z) = (2\pi R_q^2)^{1/2} e^{-z^2/2R_q^2}$$

POWER SPECTRAL DENSITY (PSD) characterises both asperity amplitude and spacing, is calculated by fourier decomposition of surface.

$$PSD(f_x) = \frac{1}{L} \left| \int_0^L f(x) e^{-2\pi f_x x} dx \right|^2$$

AUTOCORRELATION FUNCTION (ACF) is a quantitative measure of the similarity between the laterally shifted and unshifted version of the profile. It also characterizes both wavelength and amplitude properties of a surface.

$$ACF(\tau) = \frac{1}{L} \int_0^L f(x) f(x+\tau) dx$$

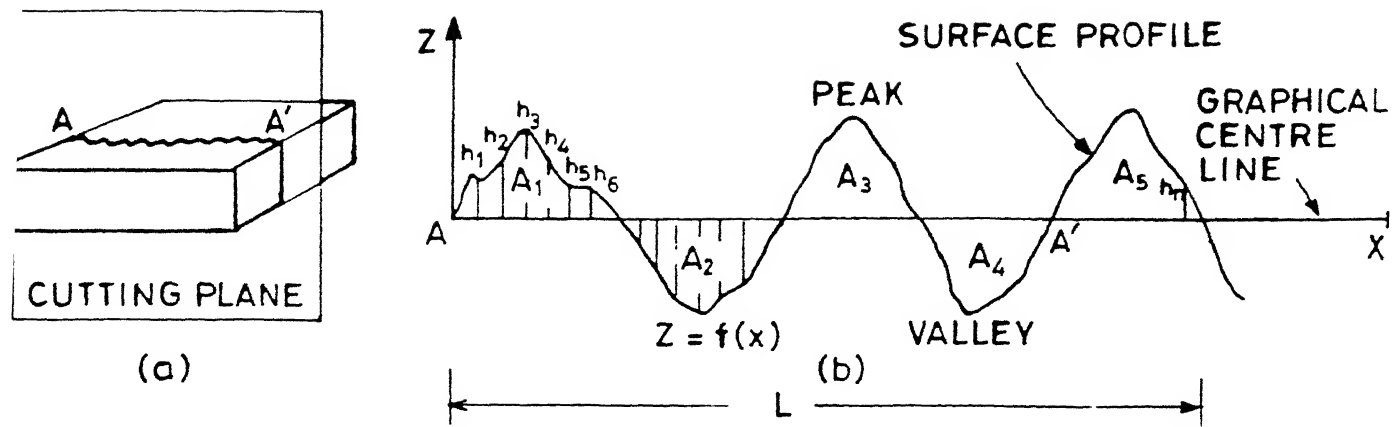


FIG. 1.4 DEFINITION OF CENTRELINE OR MEAN LINE.

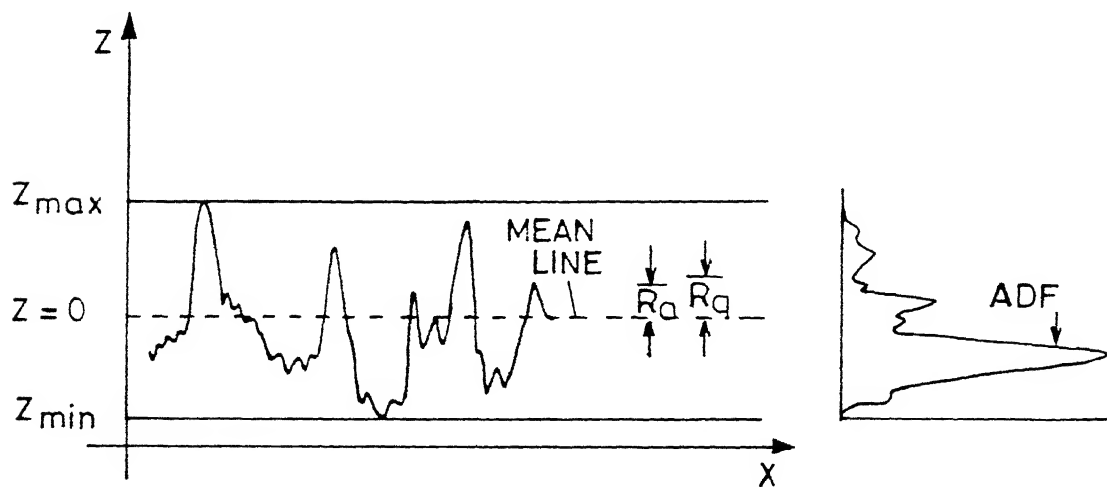


FIG. 1.5 AMPLITUDE DENSITY FUNCTION.

AVERAGE SLOPE (S_a) and RMS SLOPE (R_q) are hybrid parameters which combine both the amplitude and wavelength properties of surface.

For a continuous surface profile they can be defined as

$$S_a = \frac{1}{L} \int_0^L |df/dx| dx$$

$$S_q = \left(\frac{1}{L} \int_0^L (df/dx)^2 dx \right)^{1/2}$$

Typical value of R_a for engineering surfaces range from $0.1 \mu\text{m}$ to $10 \mu\text{m}$ and typical wavelength range from $5 \mu\text{m}$ to $800 \mu\text{m}$. Surface structures with wavelengths greater than $800 \mu\text{m}$ are classified as waviness. The R_a value produced by various processes are shown in Fig.1.6.

1.4 LITERATURE SURVEY

Measuring surface roughness by scattering of light from rough surface have been studied over years and empirical relations derived [2,3]. However no exact method is available which can cover the whole range of engineering surfaces. Stylus method still remains the conventional method for surface roughness measurement. Various techniques for the measurement of surface finish can be broadly classified into two groups [4] namely,

1.4.1 Profiling technique: In which the topographic information is derived from a point-by-point scan of surface height Z as a function of distance x along a straight line on the surface. The resulting profile is analysed by either analog or digital methods to derive roughness parameters [5]. Interferometry and stylus method come under this technique.

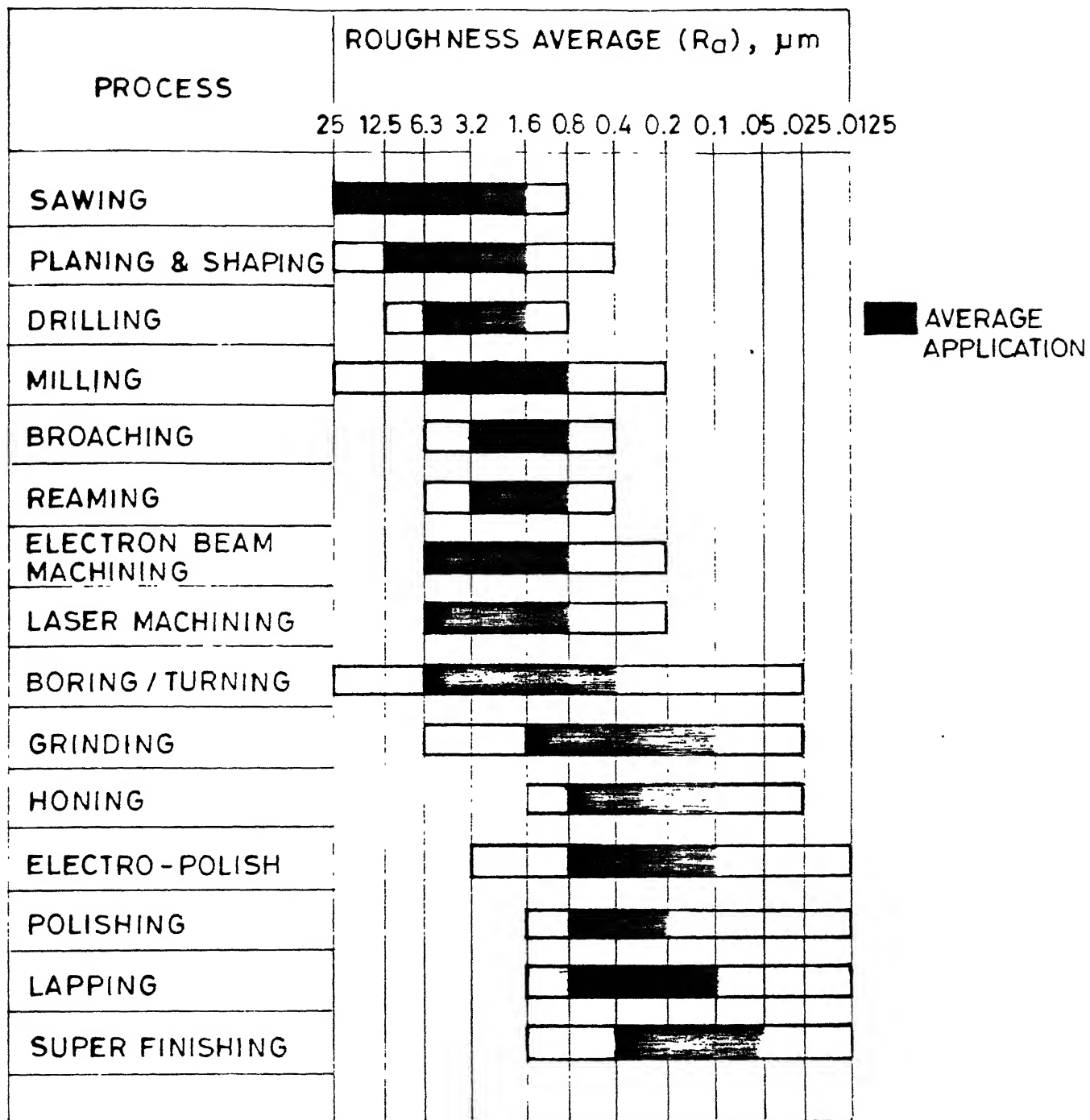


FIG. 1.6 SURFACE ROUGHNESS PRODUCED BY COMMON PRODUCTION METHODS.

1.4.1a Stylus Method: Is the most widely used and is the oldest method of measuring surface profiles. It applies same principle as that of gramophone, where a sharp probe traverses a surface and transforms its minute irregularities into electrical signal.

1.4.1b Interferometry: Is usually used to measure roughness of high-quality optical surfaces by studying the fringe pattern produced.

1.4.2 Parametric technique: The technique directly measures a parameter that represents some property of the surface topography averaged over the illuminated area. Methods like measurement of light reflected in *specular direction, total intensity of scattered light, the diffuseness of the angular scattering pattern, the speckle contrast and the polarization, to study the surface topography come under this category.

1.4.2a Specular reflectance is the method in which the light intensity scattered in specular direction (I_s) is related to R_a or R_q value of the surface [6,7,8].

1.4.2b Diffuseness of scattered light employs the ratio of intensities in specular direction to some off-specular direction and empirical relations to measure surface roughness derived for that particular surface only [2,9].

1.4.2c Speckle contrast: When a rough surface is illuminated by partially coherent light, the reflected beam consists in part of random patterns of bright and dark regions known as speckle. The

* Specular direction is the direction at an angle of reflectance equal to angle of incidence.

spatial pattern and contrast of speckle depend upon optical system, coherence condition of illumination and surface roughness of the scattering surface and is used to study surface microtopography.

1.4.2d Ellipsometry employs the measurement of change in the polarization of incident polarized light, which depends upon the composition of surface, surface structure, temperature, strain and surface roughness.

1.4.2e Angular distribution (AD): By measuring the distribution of scattered light in space around the scattering region various parameters related to roughness amplitude as well as roughness wavelength are calculated. The kind of surface information that may be obtained from AD depends upon the roughness and spatial wavelength of rough surface [4,10,11, 12].

All the above methods described in parametric technique are still in experimental stage. Although much work has been done by many researchers with positive results. Table 1.1 gives the summary of optical techniques for surface roughness measurement as taken from [4].

1.4.3 Existing theories: The relationship between scattering and surface topography is complicated and according to our survey no exact theory is available. However, full vector electromagnetic theories are available in two opposite extremes [11] namely when vertical scale of roughness is much less than the wavelength of incident light and secondly when roughness amplitude

TABLE 1.1

**SUMMARY OF OPTICAL TECHNIQUES
FOR SURFACE ROUGHNESS MEASUREMENT**

Technique	Quantitative? Capable of absolute measurements?	Can measure amplitude(A) & wavelength(W) parameters?	Speed (number of detector readings)	Horizontal resolution μm	Approximate vertical resolution μm	Vertical range of R_a μm	Surface wavelength, μm	Limits of vibration*	Can study isotropic or anisotropic surfaces?	Can study inner surfaces of parts?	Working device existing
<i>Parametric</i>											
Specular Reflectance	For $R_q < \lambda$	A	2,	~1mm	≤ 0.001	~1	0.6~100	0.1D*	Yes	Yes	Yes
tit	For $R_q < < \lambda$	A	2	~1mm	≤ 0.001	0.1	0.6~100	0.1D*	Yes	No	Yes
Diffuseness	Not yet	A	2	~1mm	~ 0.01	10	0.6~100	0.1D*	Yes	Yes	Yes
ad	For $R_q < < \lambda$	AW	10~100	~1mm	≤ 0.001	> 1	0.6~100	0.1D*	Yes	Yes	Yes
Laser Speckle Contrast	$R_q < 0.1 \lambda$	A	100	~10 λ	$\sim 10\%$ of range	0.1	0.6~100	$4\lambda/a^1$	Yes	No	No
Polychromatic	$\lambda/2 < R_q < 2I_c$	A	100	~1mm	$\sim 10\%$ of range	2~5	0.6~100	$4\lambda/a^1$	Yes	0	No
Speckle Contrast											
Speckle	$\lambda < R_q < 10\lambda$	A	10	~1mm	$\sim 10\%$ of range	1~30	0.6~100	$4\lambda/a^1$	Yes	0	No
Correlation											
Elliptometry	Not yet	-	2	~1mm	< 0.001	~1	?	?	Yes	0	No
Profiling											
Interferometry	Yes	AW	1000	2 μm	≤ 0.001	< 1	1~500	Limited by the desired resolution	Yes	No	Yes

* D* is the diameter of the detector aperture
† Q — questionable

is much greater than the wavelength of incident light. The precise condition for validity of smooth surface is given by [11,13]

$$(k_a \cos^2 \theta_i)^2 \ll 1$$

where $k = \text{propagation vector} = 2\pi/\lambda$

$\lambda = 6328.193 \text{ A}^\circ$ for He-Ne Laser

$a = \text{vertical amplitude of roughness}$

$\theta_i = \text{angle of incidence}$

$\Rightarrow a \ll 0.02 \text{ A}^\circ$ for He-Ne laser

In this limit the scattering spectrum is given by

$$\frac{1}{I_1} \left(\frac{dI}{d\omega} \right) = 4k^4 \cos \theta_i \cos^2 \theta_s \times Q \times w(p, q)$$

where $w(p, q) = \text{psd of surface roughness evaluated at spatial wave numbers } p \text{ and } q.$

and $w(p, q) = \frac{1}{A} \left| \frac{1}{2\pi} \int dx \int dy e^{i(px+qy)} Z(x, y) \right|^2$

where $Z(x, y) = \text{two dimensional surface profile}$

$A = \text{area of illuminated surface}$

$Q = \text{factor depending upon surface material and}$
 $\text{and polarization of incident light}$

$\theta_s = \text{scattering angle w.r.t. } \theta_i$

Hence the AD is direct fourier transform of surface profile $Z(x, y).$

While in the case of rough surfaces the scattering comes from surface facets. In this case the scattering spectrum is given by

$$\frac{1}{I_i} \left(\frac{dI}{d\omega} \right)_s = \frac{(1+m_x^2 + m_y^2)^2}{4\cos\theta_i} \times R \times \rho(m_x, m_y)$$

where

I_i = input intensity

$d\omega$ = infinitesimally small solid angle into which
light is scatter at θ_s

m_x and m_y are x,y components of surface slopes.

$\rho(m_x, m_y)$ is the joint surface slope probability

distribution. Hence in this case the AD directly gives the probability distribution of slopes.

In our present work however ,effort is done to measure the surface roughness by measuring AD of scattered laser light, considering the AD as diffraction pattern obtained by a periodic diffraction grating of constant amplitude and wavelength as is explained in chapter 2. Chapter 3 describes the experimental set-up, while in chapter 4 and chapter 5 experimental results and conclusion are given. The theory on which the experimental set-up is based is given in next chapter.

+ -

CHAPTER 2

THEORETICAL ANALYSIS

A rough surface scatters the collimated beam of laser light into an AD (Fig. 2.1) according to the laws of physical optics. The Intensity and pattern of AD depends upon roughness heights, spatial wavelength, wavelength of light and angle of incidence with which the light interacts with the rough surface. This AD can be seen as the diffraction pattern obtained by a periodic diffraction grating of constant amplitude and wavelength.

2.1 GENERAL SOLUTION (By Peter Beckmann [6])

Assuming that S be a continuous rough surface in 2-dimensions given by $S = Z(x, y)$, (Fig. 2.2) and a collimated beam of He-Ne laser be incident on it at an angle of incidence θ_1 w.r.t normal. The light is scattered in all directions according to the laws of physical optics. Let point of observation P be placed at an arbitrary position θ_2 w.r.t normal then,

- (1) Using cartesian coordinates (x, y, z) with origin at O, and unit vectors $\vec{x}_o, \vec{y}_o, \vec{z}_o$.
- (2) Let the rough surface be given by the function $S = Z(x, y)$, and the mean level of the surface is plane $Z = 0$.
- (3) The incident field is E_1 and the scattered field is E_2 . E_1 is assumed to be linearly polarized. Assuming E_1 to be a plane wave of unit amplitude.

$$E_1 = e^{i\vec{k}_1 \cdot \vec{r} - i\omega t}$$

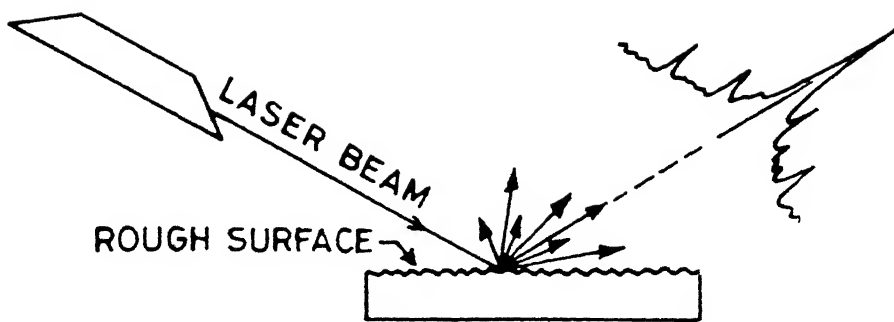


FIG. 2.1 ANGULAR DISTRIBUTION (AD) OF LIGHT SCATTERED BY A ROUGH SURFACE.

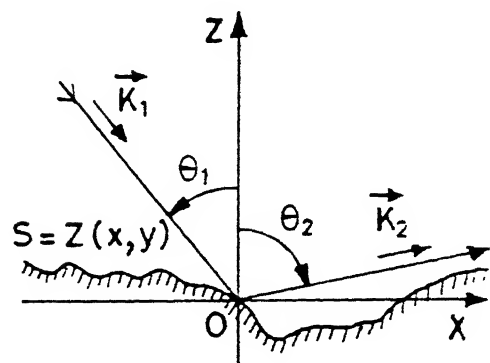


FIG. 2.2 BASIC NOTATION

where $\vec{k}_1 = \frac{2\pi}{\lambda} \frac{\vec{k}_1}{|\vec{k}|}$ = Propagation vector

$$\vec{r} = \text{radius vector} = x\vec{x}_o + y\vec{y}_o + z\vec{z}_o$$

and in particular, for points on the surface S:

$$\vec{r} = x\vec{x}_o + y\vec{y}_o + Z(x,y)\vec{z}_o$$

The angle of incidence, included between the direction of propagation of E_1 and Z axis, is denoted by θ_1 ; The scattering angle included between Z_o and \vec{k}_2 is denoted by θ_2 . Where

$$\vec{k}_2 \cong \vec{k}_1 = k = 2\pi/\lambda$$

θ_1 and θ_2 are measured in opposite senses from the +ve Z-axis. Since we are using coherent beam of light, hence the factor $e^{i\omega t}$ of $E_1 = Ae^{ik_1 \cdot \vec{r} - i\omega t}$ can be suppressed.

Now assuming origin at O, and point of incidence at S = Z(x) be a one dimensional profile (since in the present work roughness variation along y is assumed to be negligible).

Let P be the point of observation and let R' be the distance from P to a point $(x, Z(x))$ on the surface S. The scattered field E_2 at P is given Helmholtz Integral (Fig.2.3)

$$E_2(P) = \frac{1}{4\pi} \iint_S (E \frac{\partial \psi}{\partial n} - \psi \frac{\partial E}{\partial n}) ds \quad (1)$$

$$\text{where } \psi = \frac{e^{ik_2 R'}}{R'} \quad (2)$$

In order to deal with plane scattered waves, rather than spherical ones, let $R' \rightarrow \infty$ i.e. removing P to the Fraunhofer zone of

diffraction. Then

$$k_2 R' = k_2 R_0 - \vec{k}_2 \cdot \vec{r} \quad (3)$$

where R_0 = distance of P from the origin, so that

$$\psi = \frac{e^{ik_2 R_0}}{R_0} e^{-i\vec{k}_2 \cdot \vec{r}} \quad (4)$$

E and $\frac{\partial E}{\partial n}$ are the field and its normal derivative on $S = Z(x)$. And in the present case we shall assume the field E_S at any point of the surface to be field at the tangent plane on that surface.

Within the assumption we have

$$(E)_S = (1+R) E_1 \quad (5)$$

where 1 is due to incident field and R is due to reflected field and

$$(\frac{\partial E}{\partial n})_S = (1-R) E_1 \vec{k}_1 \cdot \vec{n} \quad (6)$$

n = is the normal to the surface at the considered point and R is the reflection coefficient of the smooth plane.

$R = f(\text{angle of incidence, electrical properties, polarization})$

Eq. (6) follows from

$$(H)_S = (1-R) H_1 \text{ and}$$

$$\nabla \times E = -\frac{\partial B}{\partial t} = -\mu \frac{\partial H}{\partial t}$$

$$\nu = \theta_1 - \beta = \theta_1 - \tan^{-1} \frac{\partial Z(x)}{\partial x}$$

and $\frac{\partial \psi}{\partial n} = (\nabla \psi \cdot n) = (\frac{\partial \psi}{\partial R'}) \cdot \vec{n} \quad (7)$

Substituting 4,5,6 and 7 in (1) we get

$$E_2 = \frac{ie^{ikR_0}}{4\pi R_0} \int_S (R \vec{v} - \vec{P}) \cdot \vec{n} e^{i\vec{v} \cdot \vec{r}} ds \quad (8)$$

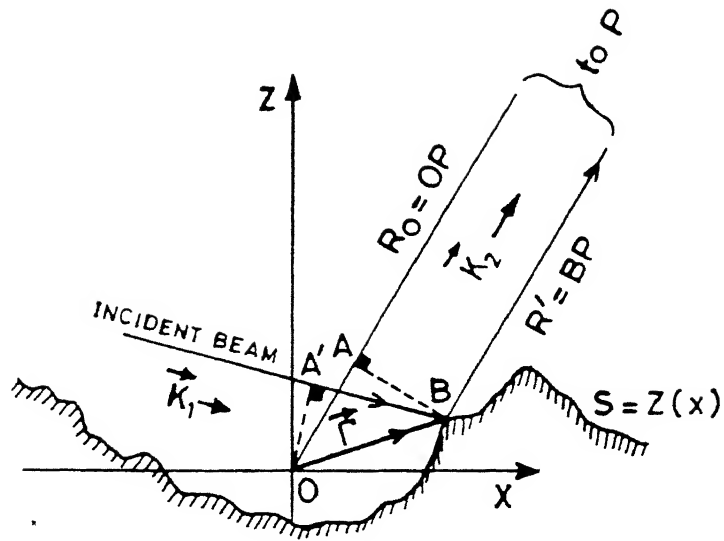


FIG. 2.3 DERIVATION OF EQUATION NO.(3)

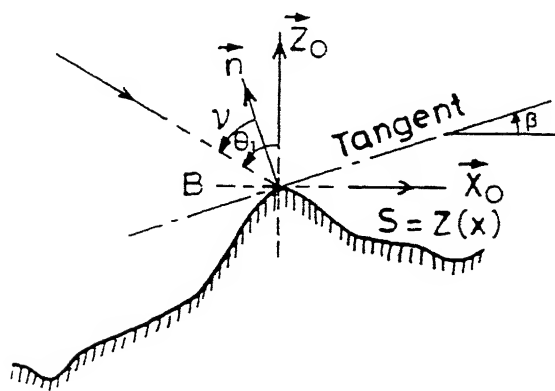


FIG. 2.4 LOCAL SCATTERING GEOMETRY

where

$$\vec{v} = \vec{k}_1 - \vec{k}_2 \quad (9)$$

$$\vec{p} = \vec{k}_1 + \vec{k}_2 \quad (10)$$

Resolving (9) and (10) into their cartesian components, we have

$$\vec{v} = k(\sin\theta_1 + \sin\theta_2)\hat{x}_o - k(\cos\theta_1 + \cos\theta_2)\hat{z}_o \quad (11)$$

$$= v_x \hat{x}_o + v_z \hat{z}_o$$

$$\vec{p} = k(\sin\theta_1 + \sin\theta_2)\hat{x}_o + k(\cos\theta_1 - \cos\theta_2)\hat{z}_o \quad (12)$$

$$\vec{n} = -\hat{x}_o \sin\beta + \hat{z}_o \cos\beta \quad (13)$$

$$\vec{r} = r \hat{x}_o + Z(x) \hat{z}_o \quad (14)$$

$$ds = \sec\beta dx; \tan\beta = \frac{\partial Z(x)}{\partial x} \quad (15)$$

For a surface extending from $x = 0$ to $x = 2L$, E_2 in scalar form can be written as

$$E_2 = \frac{ie^{ikR_o}}{4\pi R_o} \int_0^{2L} (a \frac{\partial Z(x)}{\partial x} - b) e^{iV_x x + iV_z Z(x)} dx \quad (16)$$

$$\text{where } a = (1-R)\sin\theta_1 + (1+R)\sin\theta_2 \quad (17)$$

$$b = (1+R)\cos\theta_1 - (1-R)\cos\theta_2 \quad (18)$$

To get rid of factor in front of integral in eq.no. (16) we normalize the expression by introducing the scattering coefficient

$$\rho = \frac{E_2}{E_{20}} \quad (19)$$

E_{20} = field reflected in specular direction ($\theta_2 = \theta_1$) by a smooth, perfectly conducting plane of the same dimensions under the same angle of incidence and at the same distance

$\rightarrow V_x = 0 ; Z(x) = 0, \frac{\partial Z(x)}{\partial x} = 0$ and from (16)&(18)

We find that

$$E_{20} = \frac{ik e^{i k R_0}}{\pi R_0} L \cos \theta_1 \quad (20)$$

Hence from (16) and (20) we have

ρ = scattering coefficient

$$\rho = \frac{1}{4L \cos \theta_1} \int_0^{2L} (a \frac{\partial Z(x)}{\partial x} - b) e^{iV_x x} + iV_z Z(x) dx \quad (21)$$

The integral (21) is easily integrated if a and b are assumed to be constants. One way of achieving this is to average R over the surface, making a and b independent of x (since a and b depend upon R and V). Or the other is assuming $Y = \text{CONDUCTIVITY} \rightarrow \infty$ i.e. We have a perfectly conducting plane. Defining suffix (+) for vertical polarisation and (-) for horizontal polarisation, i.e. for

VERTICAL POLARISATION $R^+ = +1$ for E_1, E_2 in plane of incidence (22)

HORIZONTAL " $R^- = -1$ for $E_1, E_2 \perp$ to plane of incidence (23)

Removing the brackets of (21) and solving the integral as product of two functions $a \frac{\partial Z(x)}{\partial x} e^{iV_z Z(x)}$ and $e^{iV_x x}$ and using the formula that

$$\int f'(x) e^{af(x)} dx = \frac{e^{af(x)}}{a}$$

where $f'(x) = \frac{\partial f(x)}{\partial x}$

we get

$$\rho = \frac{1}{4L \cos \theta_1} \left[\left(b + \frac{aV_x}{V_z} \right) \int_0^{2L} e^{i\vec{V} \cdot \vec{r}} dx - \frac{ia}{V_z} e^{i\vec{V} \cdot \vec{r}} \Big|_0^{2L} \right] \quad (24)$$

Substituting (22) and (23) in (17) and (18) we have

$$\begin{aligned} a^+ &= 2\sin\theta_2 & b^+ &= 2\cos\theta_2 \\ a^- &= 2\sin\theta_1 & b^- &= 2\cos\theta_1 \end{aligned} \quad] \quad (25)$$

Substituting these values in (24) we have

$$\rho^\pm(\theta_1, \theta_2) = \pm \sec\theta_1 \frac{1+\cos(\theta_1 + \theta_2)}{\cos\theta_1 + \cos\theta_2} \times \frac{1}{2L} \int_0^{2L} e^{i\vec{v} \cdot \vec{r}} dx + \frac{e^\pm(L)}{2L} \quad (26)$$

where

$$\rho^\pm(L) = \frac{i \sec\theta_1 \sin\theta^\pm}{k(\cos\theta_1 + \cos\theta_2)} e^{i\vec{v} \cdot \vec{r}} \Big|_0 \quad (27)$$

$$\begin{aligned} \text{with } \theta^+ &= \theta_2 \\ \theta^- &= \theta_1 \end{aligned}$$

$\vec{v} \cdot \vec{r}$ is given explicitly as

$$\vec{v} \cdot \vec{r} = \frac{2\pi}{\lambda} ([\sin\theta_1 - \sin\theta_2]x - [\cos\theta_1 + \cos\theta_2]Z(x)) \quad (28)$$

Now for the surface such that $L \gg \lambda$, II term of (26) can easily be shown to be negligible as compared to (I) term. Hence (26) reduces to simple formula

$$\rho = \frac{F_2}{2L} \int_0^{2L} e^{i\vec{v} \cdot \vec{r}} dx$$

for vertical polarization

(28)

$$\text{where } F_2(\theta_1, \theta_2) = \left(\frac{1+\cos(\theta_1 + \theta_2)}{\cos\theta_1 + \cos\theta_2} \right) \sec\theta_1 \quad (29)$$

2.2 GENERAL KIRCHHOFF SOLUTION OF THE FIELD SCATTERED BY A PERFECTLY CONDUCTING PERIODIC SURFACE

Assuming the surface S to be rough in one dimension only i.e. along x. Since $Z(x)$ is periodic of period Λ

$$\Rightarrow Z(x) = Z(x+\Lambda) \quad (1)$$

Λ = wavelength of the Roughness

The integral (26) of previous section will be periodic with period Λ if

$$V_x \Lambda = 2\pi m \text{ (where } m = 0, \pm 1, \pm 2, \dots = \text{integer}) \quad (2)$$

Since by (11) of last section

$$V_x = \frac{2\pi}{\lambda} (\sin\theta_1 - \sin\theta_2) \quad (3)$$

$$\text{We may write (2) as } \sin\theta_{2m} = \sin\theta_1 - \frac{m\lambda}{\Lambda} \quad (4)$$

which is a well known grating equation

$$\text{Let } \frac{2L}{\Lambda} = n + n_1 \text{ where } n = \text{integer}$$

$$n_1 = \text{pure fraction } (0 \leq n_1 < 1)$$

since $\int e^{i\vec{v} \cdot \vec{r}} dx$ is periodic with period Λ we may write

$$\int_0^{2L} e^{i\vec{v} \cdot \vec{r}} dx = \int_0^{\Lambda} + \int_0^{n_1\Lambda} = \frac{2L}{\Lambda} \int_0^{\Lambda} + \int_0^{n_1\Lambda} - n_1 \int_0^{\Lambda} \quad (5)$$

Substituting (2) in (27) of previous chapter we have

$$e(L) = e\left(\frac{2\pi mn_1}{V_x}\right) \quad (6)$$

Substituting (5) and (6) in (26) Section 2.1, we have for perfectly conducting, 1-dimensional periodic surface

$$\rho^\pm(\theta_1, \theta_2) = \pm \sec \theta_1 \frac{1 + \cos(\theta_1 + \theta_2)}{\cos \theta_1 + \cos \theta_2} - \frac{1}{\Lambda} \int_0^\Lambda e^{i\vec{V} \cdot \vec{r}} dx + \frac{c(n_1)}{2L}$$

$$n_1 \Lambda \int_0^\Lambda e^{i\vec{V} \cdot \vec{r}} dx \quad (7)$$

$$c(n_1) = F_2(\theta_1, \theta_2) \left[\int_0^\Lambda e^{i\vec{V} \cdot \vec{r}} dx - n_1 \int_0^\Lambda d^{i\vec{V} \cdot \vec{r}} dx \right] + e(2\pi m n_1 / V_x) \quad (8)$$

Third term of (8) is the correction term or "edge effect" which vanishes as $n_1 \rightarrow 0$ i.e. when $\frac{2L}{\Lambda}$ integral ; In any case (8) is shown to be negligible when $L \gg \Lambda$. Comparing (4) with the normal grating equation. If we calculate the path difference for the A&B rays such that they are in phase i.e. P.D. = $2\pi m$ (Fig. 2.5) We get eq.no.(4). Hence θ_{2m} correspond to the local maxima of scattered light from the rough surface. Returning to equation no.(4) we see that total no. of possible modes is limited by condition $|\sin \theta_{2m}| \leq 1$. The mode $m = 0$ is the specular mode and $m = \pm 1$ lie on either side of specular mode (Fig. 2.6) until $\theta_{2m} = \pm \pi/2$. (Mode = light scattered in the direction of maxima i.e. point at which constructive superposition of waves takes place)

Now integral (7) gives the coefficient in the direction of maxima only. Hence If we want to find out the light scattered in (any other) direction other than θ_{2m} we then return to general solution (26) of last section and neglecting the "edge effect" term we have :

$\frac{2L}{\Lambda} = n$, $n_1 = 0$. Divide $2L$ into n strips each extending from $x = j\Lambda$ to $x = (j+1)\Lambda$ where $j = 0, (n-1)$

$\Rightarrow n = \text{no. of scatterers} = \text{no. of periods present}$. Hence

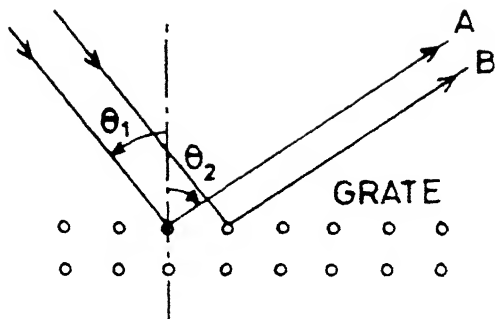


FIG. 2.5 DERIVATION OF GRATING EQUATION

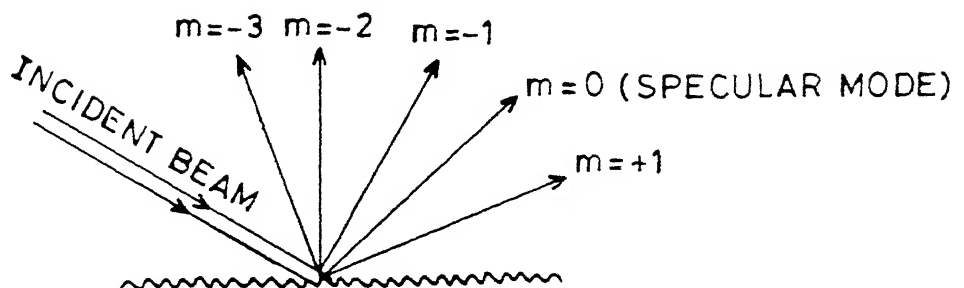


FIG. 2.6 DIRECTIONS OF SCATTERED MODES BY PERIODIC SURFACE

$$\frac{1}{2L} \int_0^{2L} e^{i\vec{V} \cdot \vec{r}} dx = \frac{1}{n\Lambda} \sum_{j=0}^{n-1} \int_{j\Lambda}^{(j+1)\Lambda} e^{iV_x x} + iV_z Z(x) dx \quad (9)$$

Since we are in Fraunhofer zone, each scatterer acts in the same manner

$$\text{Now put } V_x \Lambda = 2\pi p \quad (p = \text{any no./not necessarily an integer}) \quad (10)$$

$$\text{We have } P = \frac{\Lambda}{\lambda} (\sin \theta_1 - \sin \theta_2) \quad (11)$$

We have from (9)

$$\frac{1}{2L} \int_0^{2L} e^{i\vec{V} \cdot \vec{r}} dx = \frac{1}{n} \sum_{j=0}^{n-1} e^{i2\pi pj} \frac{1}{\Lambda} \int_0^{\Lambda} e^{i\vec{V} \cdot \vec{r}} dx \quad (12)$$

Now (12) differ from (7) by the factor

$$W = \frac{1}{n} \sum_{j=0}^{n-1} e^{i2\pi pj} = \frac{\sin(p\pi n)}{n \sin(p\pi)} \quad (13)$$

Hence the general solution for perfectly conducting periodic surface as seen at Fraunhofer zone for any scattering angle $\theta_2 =$

$$\rho^\pm(\theta_1, \theta_2) = \pm \frac{\sin(n\pi)}{n \sin(p\pi)} \sec \theta_1 \frac{1 + \cos \theta_1 + \theta_2}{\cos \theta_1 + \cos \theta_2} \frac{1}{\Lambda} \int_0^{\Lambda} e^{i\vec{V} \cdot \vec{r}} dx + O(n_1/n) \quad (14)$$

$O(n_1/n)$ = correction term which vanishes for $2L/\Lambda = \text{integral}$

2.2.1 APPLICATION TO SPECIFIC PERIODIC PROFILES

Now in our case the specimens are made on milling m/c giving high periodicity and the likely profile is to be of triangular nature. Hence solving (14) section 2.2 for a triangular profile and extending theory for more practical case.

Assuming a triangular (Δ profile) of the shown characteristics in figure 2.7. Where

$2h = \text{height}$

$$\Lambda = \Lambda_1 + \Lambda_2 \text{ wavelength/period}$$

ϕ_1, ϕ_2 = Angles depending upon tool geometry

$\phi_1 = 90^\circ - \text{effective side cutting edge angle}$

$\phi_2 = \text{effective end cutting edge angle (Fig. 4.9)}$

Now coordinates of O $\leftrightarrow (0,0)$; A $\leftrightarrow (\Lambda_1, 2h)$; B $\leftrightarrow (\Lambda, 0)$

Now

$$Z(x) = \begin{cases} OA = \frac{2h}{\Lambda_1} x; 0 \leq x \leq \Lambda_1 \\ AB = \frac{2h}{\Lambda_2} (\Lambda - x); \Lambda_1 \leq x \leq \Lambda \end{cases}$$

$$\text{and } I = \int_0^{\Lambda} e^{iV_x x + iV_z z} Z(x) dx \text{ of (14)} = \int_0^{\Lambda_1} e^{iV_x x + iV_z z} Z(x) dx + \int_{\Lambda_1}^{\Lambda} e^{iV_x x + iV_z z} Z(x) dx$$

$$\frac{I_1}{I_2}$$

$$I_1 = \int_0^{\Lambda_1} e^{i\vec{V} \cdot \vec{r}} dx = \int_0^{\Lambda_1} e^{iV_x x + \frac{i2hV_z}{\Lambda_1} x} dx = \int_0^{\Lambda_1} e^{i(V_x + \frac{2hV_z}{\Lambda_1})x} dx$$

$$= \left(\frac{2}{C_1} \sin C_1 \frac{\Lambda_1}{2} \right) * e^{iC_1 \frac{\Lambda_1}{2}} = R_1 e^{i\mu_1} \quad (15)$$

$$\text{where } C_1 = V_x + \frac{2hV_z}{\Lambda_1} \quad (15a)$$

$$R_1 = \frac{2}{C_1} \sin(C_1 \frac{\Lambda_1}{2}) \quad (15b)$$

$$\mu_1 = C_1 \frac{\Lambda_1}{2} \quad (15c)$$

$$I_2 = \int_{\Lambda_1}^{\Lambda} e^{iV_x x + iV_z \frac{2h}{\Lambda_1}} \Lambda - iV_z \frac{2hx}{\Lambda_2}$$

$$= e^{iV_z \frac{2\Lambda h}{\Lambda_2}} \int_{\Lambda_1}^{\Lambda} e^{i(V_x - \frac{2hV_z}{\Lambda_2}x)} dx = R_2 e^{i\mu_2} \quad (16)$$

$$R_2 = \frac{2}{C_2} \sin(C_2 \frac{\Lambda_2}{2}) \quad (16a)$$

$$\mu_2 = 2hV_z \frac{\Lambda}{\Lambda_2} + C_2 \Lambda_1 + (C_2 \Lambda_2 / 2) \quad (16b)$$

$$C_2 = V_x - 2V_z \frac{h}{\Lambda_2} \quad (16c)$$

$$I = I_1 + I_2 = R_1 e^{i\mu_1} + R_2 e^{i\mu_2} = R e^{i\mu} \quad (17)$$

$$\text{Where } R^2 = R_1^2 + R_2^2 + 2R_1 R_2 \cos(\mu_1 - \mu_2) \quad (17a)$$

$$\& \tan \mu = \frac{R_1 \sin \mu_1 + R_2 \sin \mu_2}{R_1 \cos \mu_2 + R_2 \cos \mu_2} \quad (17b)$$

2.2.1a I CONSIDERATION

Assuming detector is at Fraunhofer Zone put (17) in (14) to get general distribution of light amplitude at Fraunhofer zone

$$\rho = (W * F * \frac{R e^{i\mu}}{\Lambda}) \quad (18)$$

$$\text{where } W = \frac{\sin(np\pi)}{n \sin(p\pi)}, F = \sec \theta_1 \frac{1 + \cos(\theta_1 + \theta_2)}{\cos \theta_1 + \cos \theta_2}; R \& \mu \text{ are given by}$$

(17a) and (17b) of section 2.2.1 respectively

2.2.1b II CONSIDERATION

Now, in practice it is not possible to put the detector in the Fraunhofer Zone to measure angular distribution. Hence for a periodic surface, the total field scattered into a certain

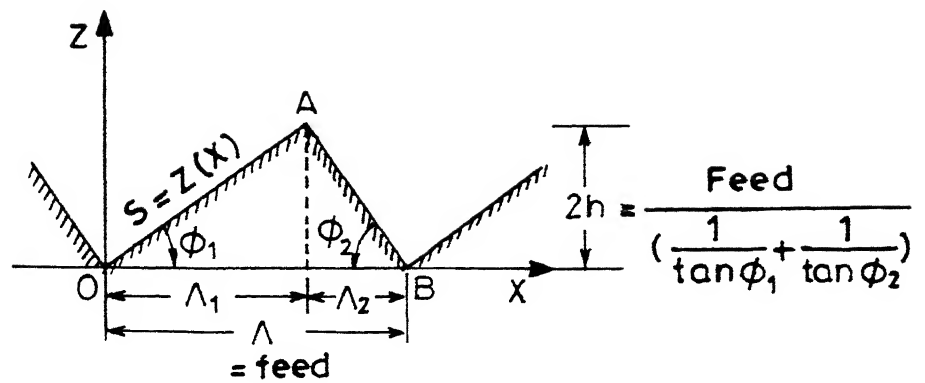


FIG. 2.7 PROFILE SPECIFICATIONS.

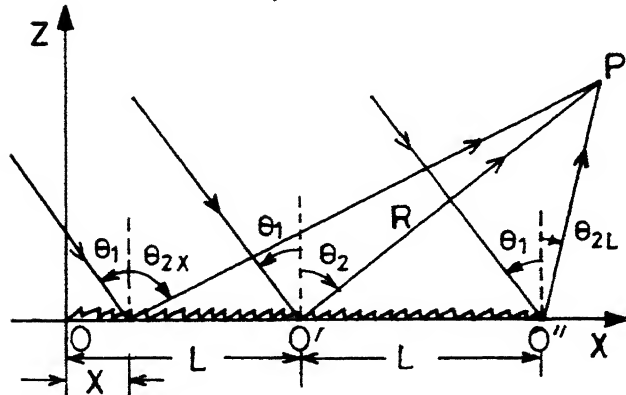


FIG. 2.8 FIELD AT ANY POINT P IN FRESNEL ZONE IS SUM OF AMPLITUDES SCATTERED BY DIFFERENT WAVE PERIODS.

direction is given by adding the contributions of each period to that direction (Fig.2.8). Now since in this kind of situation θ_2 has a weak dependence x . Hence v_x, v_z, C_1, C_2 vary along the x hence we return to general solution (21) of last chapter and assuming $\theta_2 = \text{constant}$ for $x = j\Lambda$ to $x = (j+1)\Lambda$ for $j = 0, (n-1)$ we have 'a' and 'b' of last section 2.1 eq. (17) & eq.(18) also constant \rightarrow

$$\rho = \frac{1}{4L\cos\theta} * \int_0^{\Lambda} (a \frac{\partial Z(x)}{\partial x} - b) e^{iv_x x + iv_z Z(x)} dx \quad (19)$$

O' = Reference point & $O'P = R'$

$$\theta_{2x} = \tan^{-1} \left(\frac{x-L}{R\cos\theta_2} \right) \quad (20)$$

breaking (19) for each scatterer we have

$$\rho = \frac{1}{4L\cos\theta_1} * \left[\int_0^{\Lambda} (\) dx + \int_{\Lambda}^{2\Lambda} (\) dx + \dots + \int_{j\Lambda}^{(j+1)\Lambda} (\) dx + \dots + \int_{(n-1)\Lambda}^{n\Lambda} (\) dx \right] \quad (21)$$

taking j^{th} integral we have

$$\rho_j^{\text{th}} = \frac{1}{4L\cos\theta_1} * \int_{j\Lambda}^{(j+1)\Lambda} (a \frac{\partial Z(x)}{\partial x} - b) e^{iv_x x + iv_z Z(x)} dx \quad (22)$$

Since a, b, v_x and v_z are i.e θ_2 is assumed to be constant between one wave period. Hence solving (22)

Just like (21) of previous chapter we have

$$\rho_{j,\text{th}} = F_j * e^{i2\pi P} \int_0^{\Lambda} e^{iV_x x} + iV_z Z(x) dx \quad (23)$$

$$F_j = \sec \theta_1 \frac{1 + \cos(\theta_1 + \theta_{2x})}{\cos \theta_1 + \cos \theta_2} * \frac{1}{2L} \quad (24)$$

$$\text{and } \int_0^{\Lambda} e^{iV_x x} + iV_z Z(x) dx = R_j e^{i\mu_j}$$

since θ_2 varies for each j as x varies from

$$x = 0*j = 0 \text{ to } x = n_j = 2L$$

Hence $(n-1)$

$$\rho = \sum_{j=0}^{n-1} (F_j * e^{i2\pi P j} * R_j e^{i\mu_j}) \quad (25)$$

Where R_j and μ_j are found from (17a) & (17b) by substituting θ_{2x} for θ_2 ; where θ_{2x} is given by (20).

2.3 OBSERVATIONS

Now the intensity scattered by a periodic rough surface in any direction θ_2 is given by eq. no. 18 section 2.2 as,

$$\rho = W * F * \frac{R}{\Lambda} e^{i\mu}$$

where R and μ are given by (17a) and (17b) of section 2.2., W by (13) section 2.2 and F by (29 section 2.1). Now for simplicity assuming that the point P of observation is placed in specular direction i.e. in that case $\theta_1 = \theta_2$ then observing the variations in specular intensity.

$$\text{Now for } \theta_1 = \theta_2 \quad (1)$$

$$\Rightarrow V_x = k (\sin \theta_1 - \sin \theta_2) = 0 \quad (2)$$

$$\text{and } P = \frac{\Lambda}{\lambda} (\sin \theta_1 - \sin \theta_2) = 0 \quad (3)$$

Hence $W = F = 1$ and putting (1)&(2) in (15a,b,c) and (16a,b,c) of section 2.2.1, we get

$$C_1 = -C_2 = 2V_z \frac{h}{\Lambda_2}$$

$$\text{and } \mu_1 = \mu_2 = V_z h$$

$$\text{Hence } R^2 = (R_1 + R_2)^2 = * \text{sinc}^2(V_z h) \quad (4)$$

$$\text{where } V_z = 2k \cos \theta_1 = 2k \cos \theta_2$$

Hence intensity variation in specular direction is given by (4) i.e.

$$I_s = \text{sinc}^2(V_z h) \quad (5)$$

2.3.i Variation of θ_1 = angle of incidence

Now Re-writing (4)

$$I_s = \text{sinc}^2(2kh \cos \theta_1) = f(\theta_1) \quad (6)$$

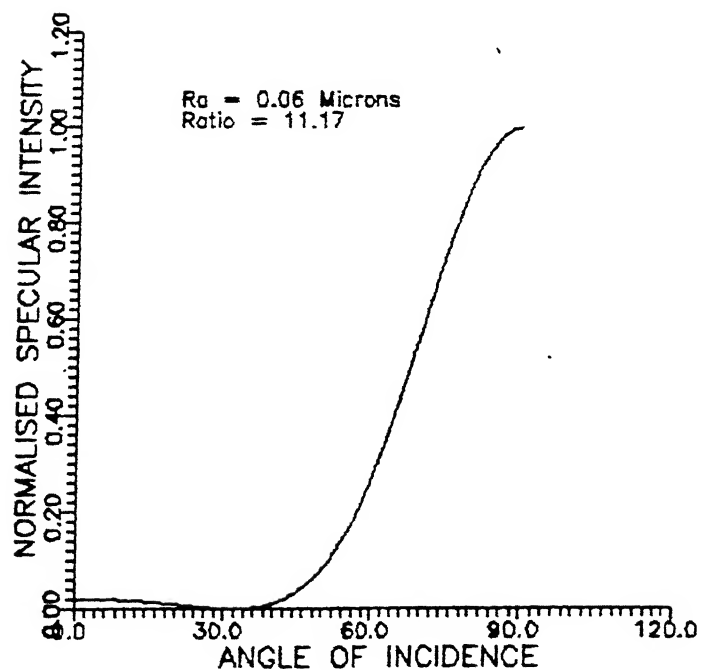
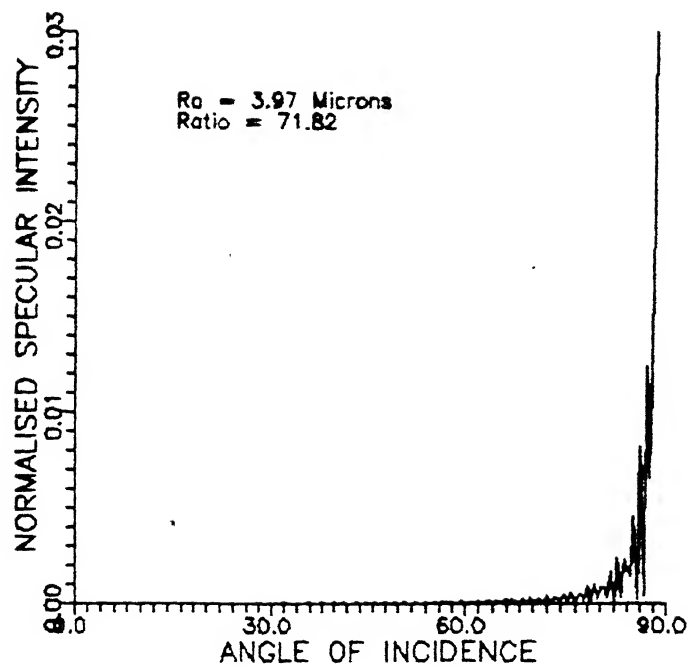
Now as θ_1 goes on increasing the value I_s goes through a periodic function and at near grazing angle of incidence

$$\begin{aligned} \theta_1 &\rightarrow 90^\circ \\ I_s &\rightarrow 1 \end{aligned} \quad (7)$$

Eq. (7) is a standard result i.e. at near grazing angle of incidence even the rough surfaces reflect specularly **. Hence (7) justifies our theory also. The variation of I_s is plotted theoretically for two surfaces having different values of h or in other words, different values of R_a (Fig. 2.9).

$$*\text{sinc}x = \frac{\sin x}{x}$$

** Phenomenon of Road glare



A look at the graphs show that for a smooth surface the light reflected in specular direction increases smoothly with increasing angle of incidence, while for a comparatively rough surface the variation is rather abrupt.

A look at eq. (4) shows that the light reflected in specular direction is independent of the spatial wavelength of the roughness. Hence it can be utilised as a strong tool to measure the Ra value of rough surfaces

2.3.2 Variation of h : Now if we keep θ_1 constant and try to see the effect on I_s by the variation of h i.e.. The roughness amplitude, we have

$$I_s = \text{sinc}^2(V_z h) \quad (8)$$

Hence as $h \rightarrow 0$ i.e. approaching a perfectly smooth surface

$$I_s \rightarrow 1 \quad (9)$$

Hence a perfectly smooth surface reflects all the incident light in specular direction which is logically true also. Hence Eq. (9) confirms that the theory is correct. Fig.(2.10) show the variation of specular intensity vs roughness amplitude for two angles of incidence. Figure shows that light scattered in specular direction goes on decreasing with increase in roughness of the surface.

2.3.3 Theoretical Angular distribution (ADD) According to eq.(4) section 2.2.1 the scattering pattern consists of finite

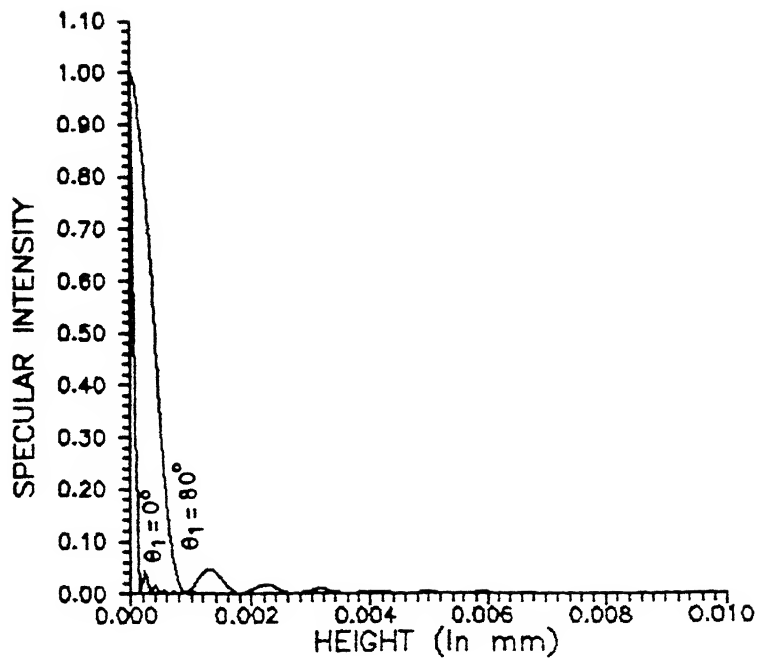


FIG. 2.10. VARIATION OF SPECULAR INTENSITY WITH ROUGHNESS HEIGHT (h)

diffraction spots at discrete angles, when the scattering pattern is obtained by perfectly conducting periodic surface and the no. of diffraction spots depend upon the ratio :

$$r = \frac{\Lambda}{\lambda} \quad (10)$$

That is larger this ratio more the no. of scattered modes. The no. is given by

$$N = 2r+1 \quad (11)$$

And the intensity propagated in each mode is given by (25) section 2.2.1b and the angle at which a particular mode is propagated or a diffraction spot is obtained is given by

$$\theta_{2m} = \sin^{-1} (\sin \theta_1 - \frac{m\lambda}{\Lambda}) \quad (12)$$

m = +ve or -ve integer

m = 0 for specular mode

where max. and min. value of m is obtained by putting $\sin(\theta_{2m}) = +1$ and -1 respectively

For example, for a surface having ratio * r = 11.58 the total no. of scattered modes is

$$(2r+1) = 24.176$$

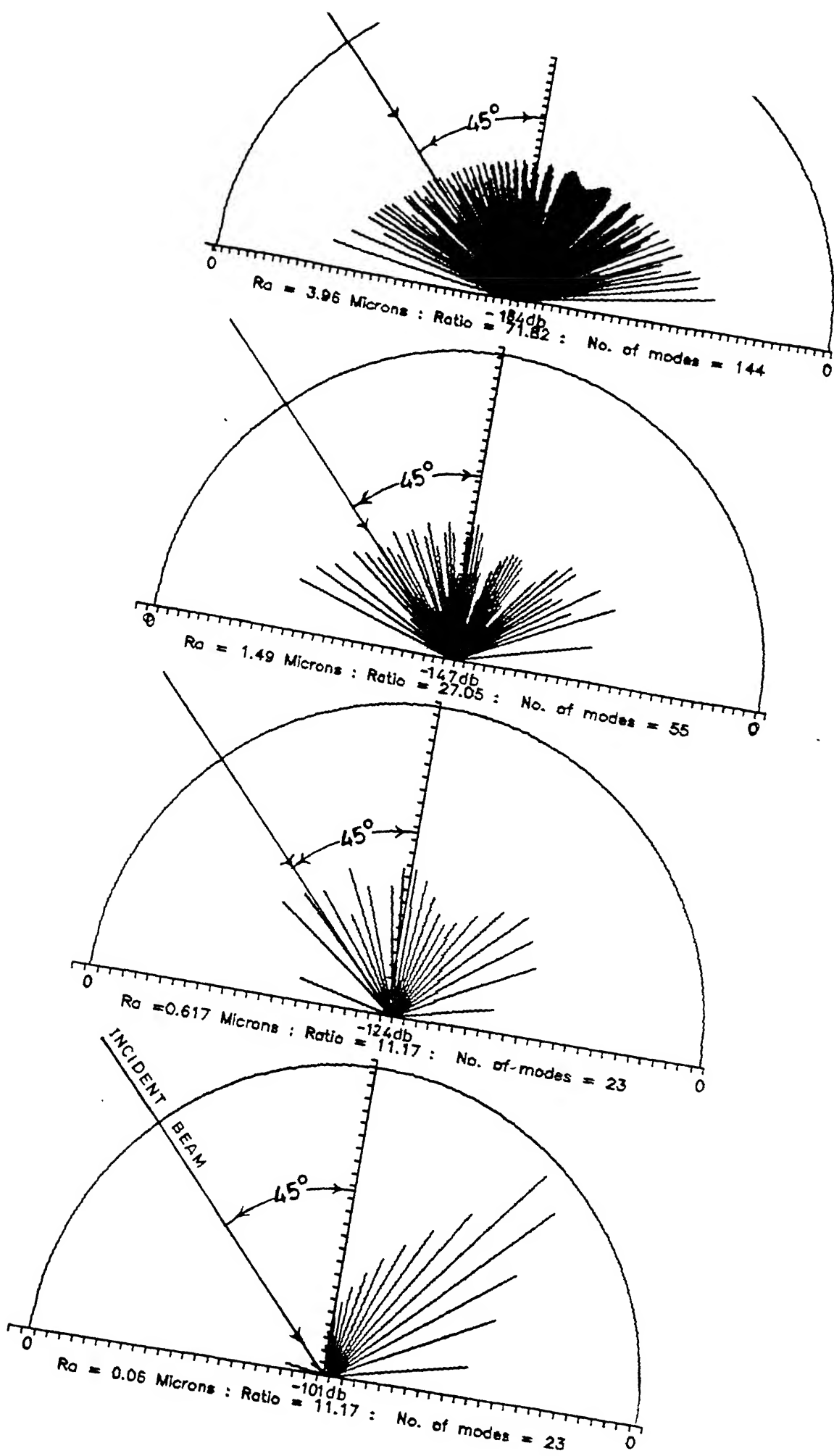
Since the fractional part has no significance hence

$$N = 24$$

Fig (2.11) shows the theoretical scattering pattern by a triangular surface.

But according to [11] each surface is a superposition of both random as well as periodic roughness. Hence the presence of

* = 11.58 corresponds to f = 22mm/min and R.P.M. = 3000 on milling n



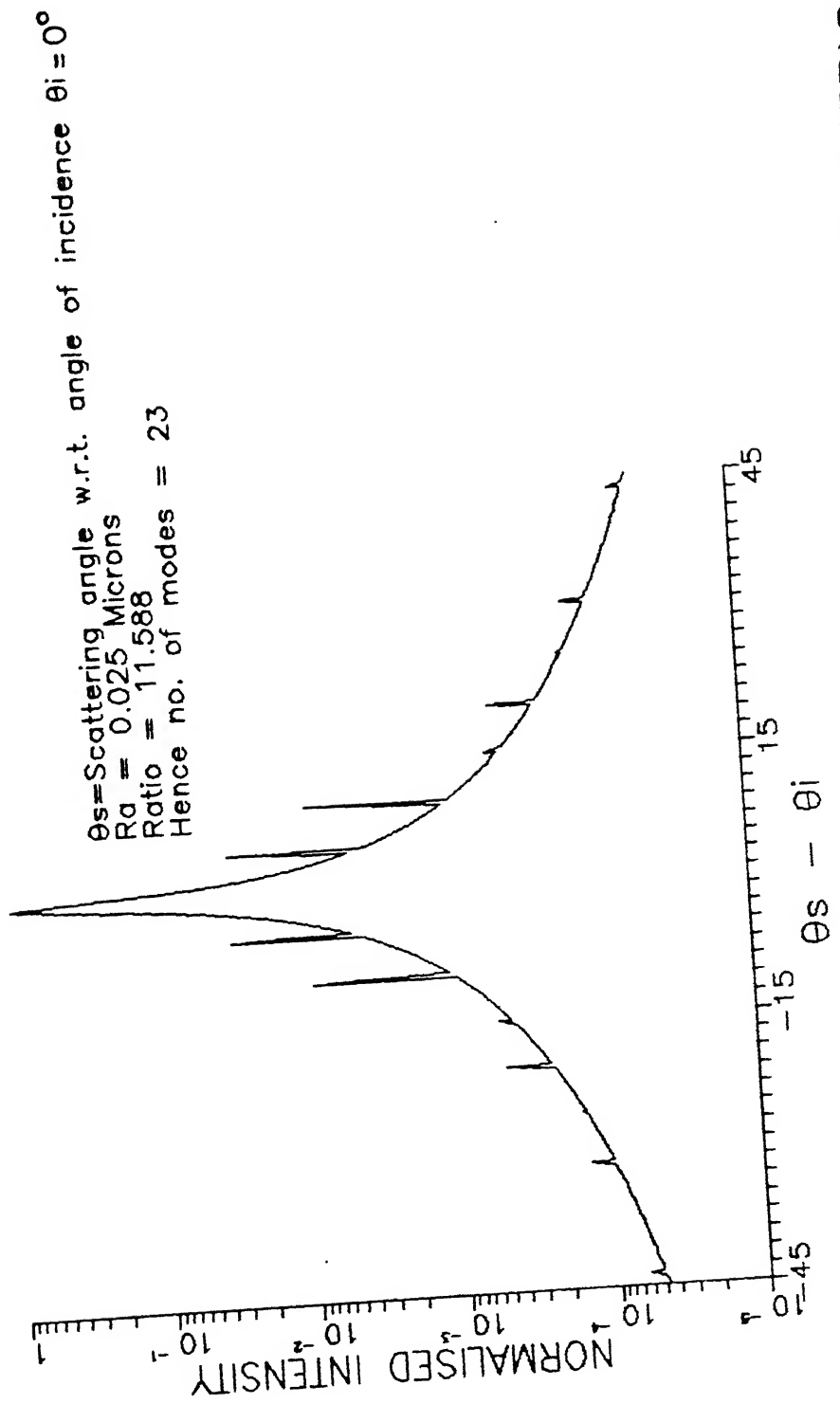


FIG. 2.12

THEORETICAL AD FOR A TRIANGULAR SURFACE

random one - dimensional component the total intensity falls off as the second power of scattering angle away from the specular direction. Hence the likely AD pattern to be obtained is shown in figure 2.12.

2.3.4 Separation of modes :

Figure 2.13 shows the angular difference between two adjacent modes for different values of spatial wave length Λ . The symmetry of the plots show that the modes are symmetrically placed and the angular separation is constant for in between modes. Hence by measuring their angular difference it may be possible to predict the spatial wavelength of the surface roughness. Table (2.1) gives the theoretical separation between modes for different values of spatial wavelength.

2.4 Conclusions :

By variation of different parameters the following conclusions come forward

(a) Light reflected in specular direction goes on decreasing with increase in surface roughness.

(b) At near grazing angle of incidence all the surfaces tend to reflect specularly.

c) larger spatial wavelength components diffract light into smaller angles while smaller spatial wavelength components diffract light into larger angles

And a final conclusion that the roughness is a relative term when compared with wavelength of incident light. Which is evident if we re-write (31) as

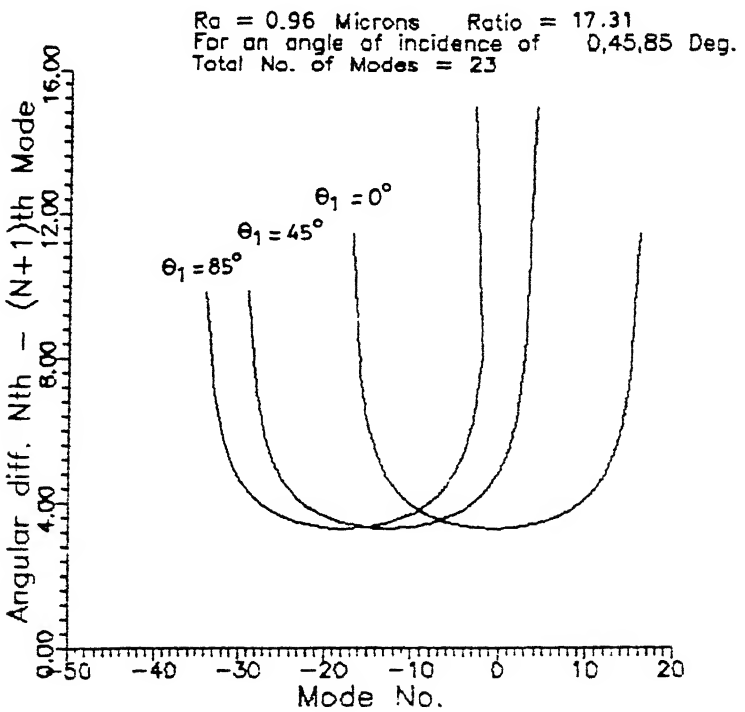
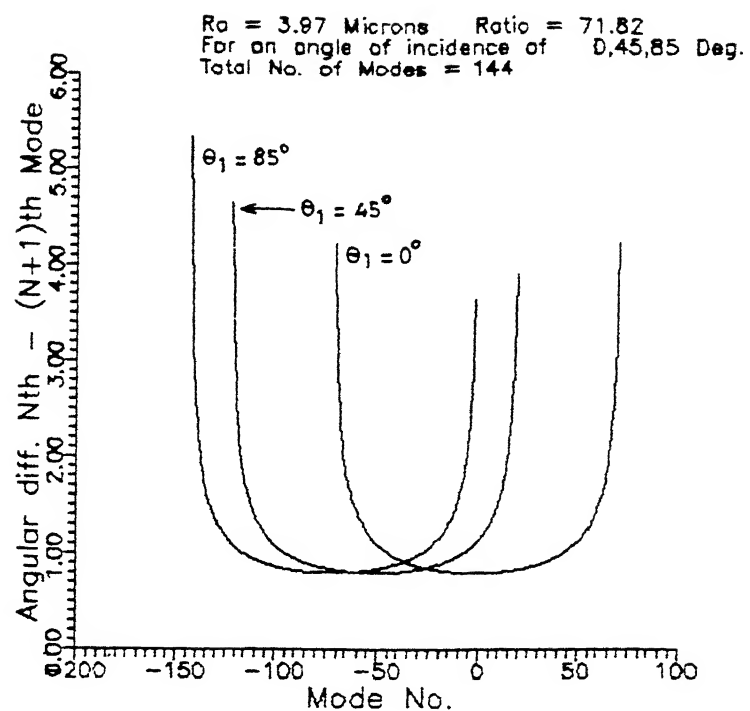


FIG. 2.13

THEORETICAL SEPARATION OF MODE

TABLE 2.1
MODE SPECIFICATIONS

Specimen No.	Ratio Λ/λ	Theoretical Separation of modes (deg.)	Theoretical No. of modes	Average Expt. spacing
FA-1	2522	0.022°	5045	2.2°
FA-2	1008.1	0.056°	2017	2.3°
FA-3	314	0.18°	629	2.67°
FA-4	77.43	0.74°	155	2.926°
MA-1	17.31	3.3°	35	
MA-2	34.63	1.6°	70	
MA-3	107.62	0.53°	216	
MA-4	68.19	0.84°	137	
MA-5	71.82	0.79°	144	3.15°
MA-6	27.05	2.1°	55	
MA-7	11.17	5.1°	23	
MA-8	17.464	3.28°	35	
MA-9	27.33	2.09°	55	
MA-10	17.31	3.3°	35	
MA-11	11.17	5.1°	23	

$$I_s = \text{sinc}^2\left(2*\frac{2\pi}{\lambda}*\cos\theta_1*h\right) = \text{sinc}^2\left(\epsilon \frac{h}{\lambda}\right) = f\left(\frac{h}{\lambda}\right)$$

where $\epsilon = 4\pi\cos\theta_1$ = constant

Keeping h constant and varying λ we see that for $\lambda_1 > \lambda_2$

$$I_{s1} > I_{s2}$$

which shows light with larger wavelength sees a surface as a smooth one which on the other hand may be rough for light with smaller wavelength. For example the radio waves are simply reflected specularly by clouds, trees, houses etc. while the sunlight is totally scattered or diffused.

2.5 ASSUMPTIONS

The assumption used while deriving (28) section 2.1 and (7) section 2.8 are :

- (A) The surface is perfectly conducting and quantities a and b in (17), (18) section 2.1 are constant.
- (B) Mutual interaction of irregularities (shadowing or multiple scattering) may be neglected
- (C) The incident plane wave is linearly polarized
- (D) The point of observation is sufficiently far removed from the surface to regard the scattered waves as plane waves.
- (E) Field at any point on the surface is expressed as sum of the incident and reflected field where R is the reflection coefficient of the plane tangent at the considered point ((5), section 2.1)

Assumption (E) implies that the surface undulations should be smooth and there should be no sharp corners. Hence in the present case of a triangular profile the theory is not applicable to the points O, A and B. Fig.2.7

CHAPTER 3

EXPERIMENTAL SET-UP AND PROCEDURE

In the present work effort is done to relate the AD of scattered light to surface microtopography. To perform the experiment few things such as a laser, photo-detector, a rough surface, multimeter and a AD measuring instrument are necessary. Due to non-availability of any instrument for measuring AD a new one had to be designed and fabricated. Measurement of AD requires that the rough surface specimen be kept fixed w.r.t laser while the detector rotates about the point of incidence on the rough-surface specimen. Since AD depends upon the angle of incidence also, a provision for change of angle of incidence is also necessary. To achieve the above two motions following requirements came forward and their solutions were found, which crystallised into the instrument shown in Fig.3.1.

Some of the salient features of the instrument are (Fig.3.1):

- a. Three rotational and one translational motion along Z-axis for the detector
- b. One translational motion along Y-axis for the whole system
- c. Two translational motion along Z and Y-axis and one rotational motion about Z-axis for the specimen
- d. Minimum rotational motion possible for the detector with hand is 0.1 degrees
- e. An unconventional method of measuring AD, in which detector is kept fixed while the specimen rotates [11], is also possible with this system.

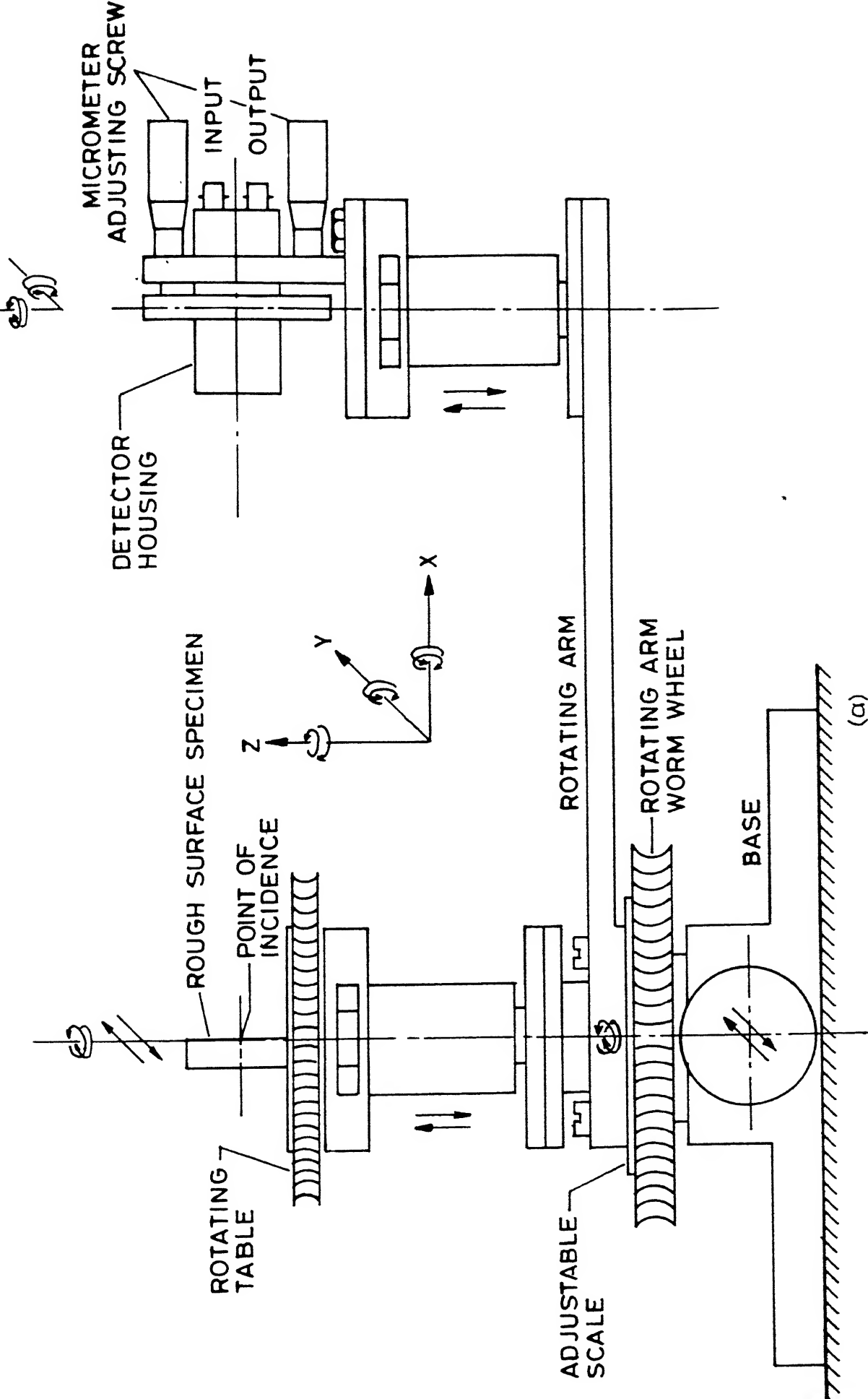
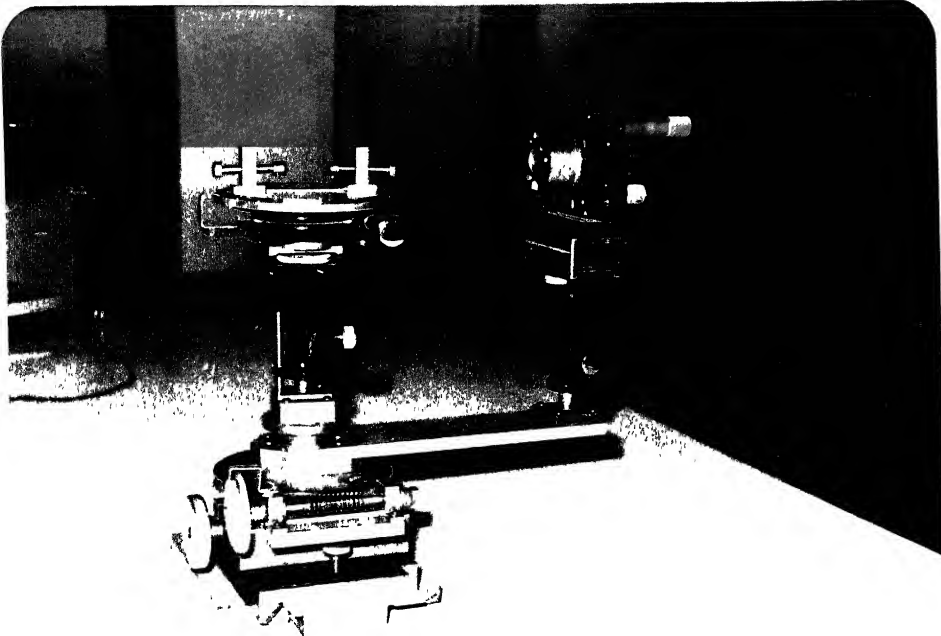
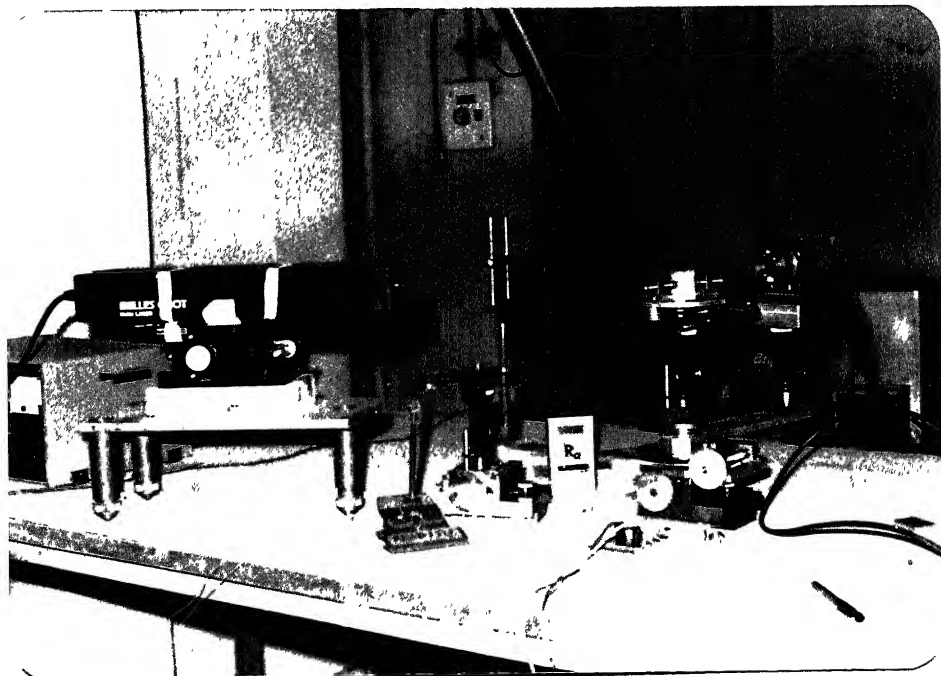


FIG. 3.1 SCATTERED INTENSITY MEASURING INSTRUMENT.
(a)



(b)



(c)

FIG. 3.1 (CONTD.)

3.1 EXPERIMENTAL SET-UP

Following steps are taken before setting up the experiment:

3.1.1 Selection of laser: Scattering of light from a rough surface depends upon the angle of incidence and wavelength of light source. Furthermore light is scattered in all directions, hence an intense source of light is desirable so that light scattered in a particular direction is of measurable amount. Laser is a source of highly monochromatic and intense beam of light. Combined with its directionality, it is the ideal light source for the experiment. A 5mW 'Melles-Griot' He-Ne laser polarised in the plane of incidence, $\lambda = 6328.193 \text{ \AA}^{\circ}$, is used in the experiment (Fig.3.1-c). Since He-Ne lasers are commercially available and their wavelength lies in the visible range, hence their applicability in the present work.

3.1.2 Selection of photo-detector: C30808 P-i-N phototransistor (Fig.3.4) sensitive to He-Ne laser wavelength with the specifications given in Table 3.1 is used for experimentation. Responsivity of detector is calibrated experimentally (Fig.3.2). The detector housing is designed (Fig.3.5) incorporating an amplifier circuit (Fig.3.3). Care is taken that the detector output does not exceed the saturation voltage of 47.3V while performing an experiment. Assuming that intensity falling on the detector is constant over its entire sensitive area for any scattering direction θ_s w.r.t. θ_i , the output of detector is proportional to the intensity of scattered light. The solid angle subtended by detector on the rough surface needs to be small so as to allow minimum diffused light and large enough so as to receive all the light scattered in a particular direction.

Table 3.1

PHOTODIODE SPECIFICATIONS

Part No.	Photosensitive surface Area Dia	Typical spectral response range 10% point	Maximum Ratings				Field of view (degree)	
			D.C. Reverse voltage	Photocurrent density I_p	Forward current I_F			
			V_{PM}	Av. DC Valve	Peak Valve	Av. DC Valve		
308	5 mm ²	nm	V	mA/mm ²	mA/mm ²	mA	mA	mA
308	5	2.5	400 to 1100	100	5	20	10	100
								72

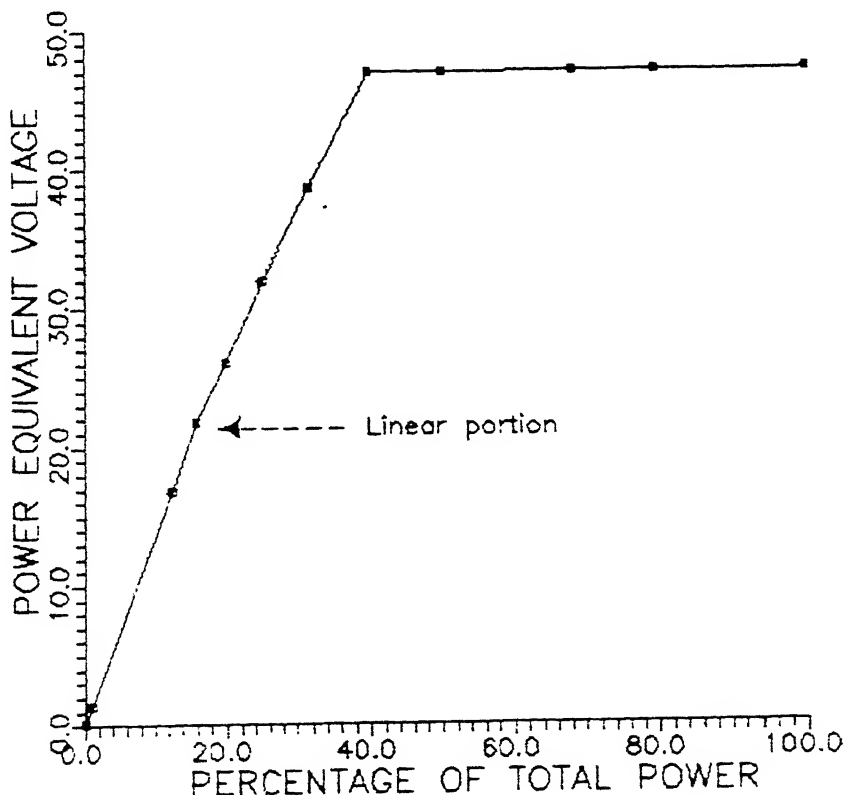


FIG 3.2

PHOTODIODE RESPONSIVITY CURVE

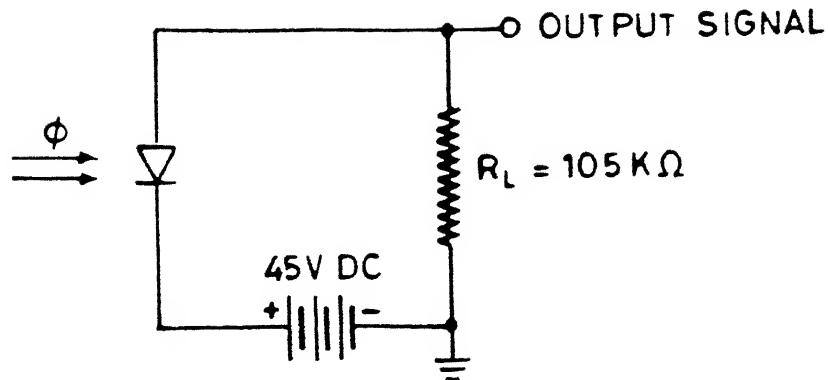
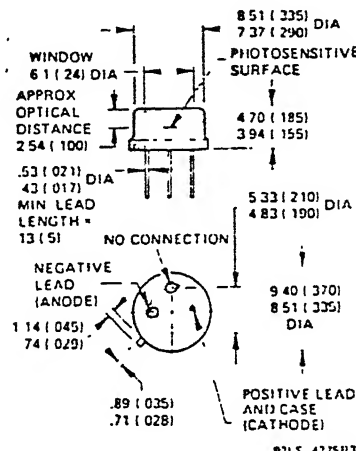


FIG. 3.3 AMPLIFIER CIRCUIT

C30808



Dimensions in millimeters. Dimensions in parentheses are in inches

FIG. 3.4 C 30808 PHOTOTRANSISTOR.

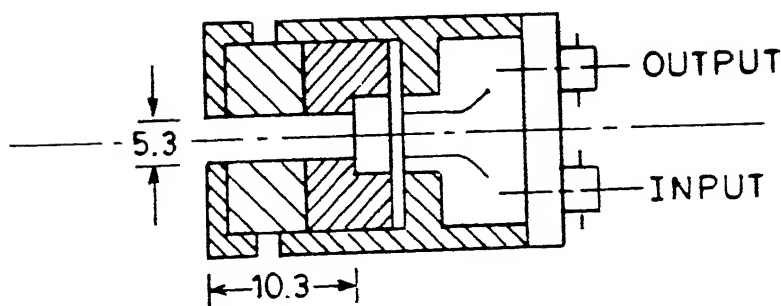


FIG. 3.5 X-SECTION OF DETECTOR HOUSING.

(Fig.3.6).

P' = Point of incidence on specimen

DD' = detector sensitive area = 2.5mm dia

RR = distance of detector from specimen = 230mm

$$\text{solid angle subtended } \theta = \frac{\pi(DD')}{2(RR')^2} = \frac{\pi(2.5)^2}{4*52900} = 0.0001 \text{ steradians}$$

Total surface VV' viewed by detector (Fig.3.7)

$$= \frac{2rR}{x} = \frac{5.3 \times 230}{10.34} = 117.8 \text{ mm} > \text{laser spot size on the surface}$$

3.1.3 Detector motion: Intensity is the rate of flow of energy per unit area and in case of scattering the intensity in a particular direction goes on decreasing with distance, because the scattered light expands in space. Hence the detector is required to move in a radius about the point of incidence, so as to measure intensity at the same distance from the point of incidence. Hence detector is mounted at the end of a rotating arm whose axis of rotation coincides with the axis of rotation of rotating table on which rough surface specimen is mounted.

3.1.4 Point of incidence: Angular distribution of scattered light can change with the point of incidence on the rough surface specimen. Hence the point of incidence on the rough surface specimen should coincide with the centre of rotation of rotating table on which the specimen is placed (Fig.3.1). Else the point of incidence changes as the incidence angle is changed. This is

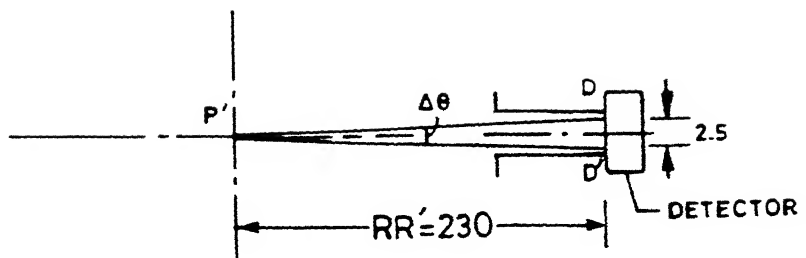


FIG. 3.6 SOLID ANGLE SUBSTENDED BY DETECTOR.

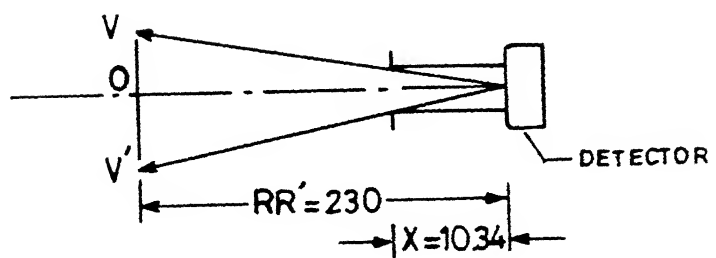


FIG. 3.7 SURFACE VIEWED BY DETECTOR.

also shown geometrically for two possible cases, namely, when point of incidence does not coincide with centre of rotation of specimen, centre of rotation of specimen coincides with centre of rotation of rotating table (Fig. 3.8-b). Then point of incidence changes by

$$\delta = AC - AB = r \frac{\cos(\theta_i - \alpha) - \cos\theta_i}{\cos(\theta_i - \alpha)}$$

and secondly, when, centre of rotation of specimen does not coincide with centre of rotation of rotating table (Fig 3.8-c)

$$\text{Change} = AB = r \frac{\tan \alpha \cdot \cos(\alpha - \theta_i) - (\sec \alpha - 1)\sin \theta_i}{\cos(\alpha - \theta_i)}$$

r = radius eccentricity

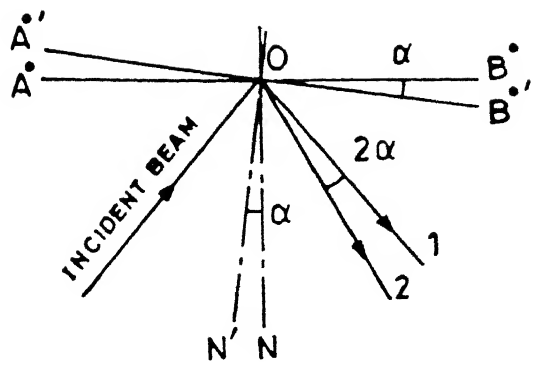
θ_i = angle of incidence

α = change in angle of incidence

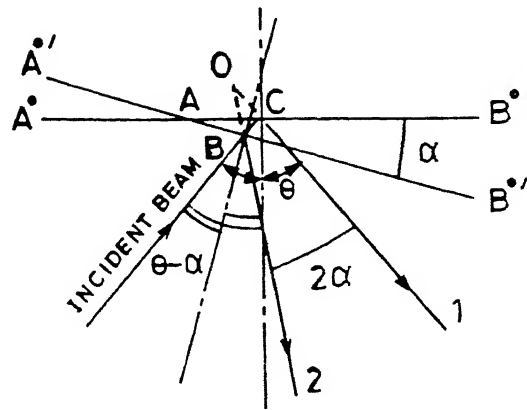
The motion of both specimen and detector is achieved by worm and worm wheel arrangement designed by Lewis equation and are fabricated outside Kanpur.

3.1.5 Need for vertical motion (Fig. 3.1): It is observed that for highly periodic surface the light is scattered perpendicular to the direction of *lay at the point of incidence. Since the detector rotates in horizontal plane only. Hence need of vertical motion along Z-axis for the specimen is required so as to make scattered pattern horizontal (Fig. 3.12-a) by changing the point of incidence. Also a horizontal motion along Y-axis is incorporated so as to make scanning of whole rough surface possible by combination of motion along Y and Z-axis. Detector vertical motion is also desired so that the detector properly accepts the scattered intensity pattern.

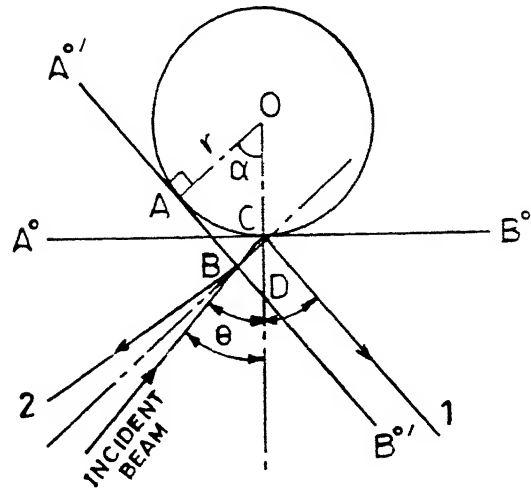
* In the present work the lay of the rough surface specimens (rss) has a circular curvature.



(a) POINT OF INCIDENCE = POINT OF ROTATION
 AB° = SPECIMEN SURFACE



(b) POINT OF INCIDENCE \neq POINT OF ROTATION



(c) POINT OF ROTATION NOT ON SPECIMEN SURFACE

FIG. 3.8 EFFECT ON POSITION OF POINT OF INCIDENCE WITH CHANGE IN ANGLE OF INCIDENCE BY ROTATING THE SPECIMEN.

scattered intensity pattern.

3.1.6 Mirror mounts: The detector should be perpendicular to the surface of the specimen at the point of incidence. Hence the detector housing is mounted on mirror mount and initial adjustment is done by replacing the specimen by mirror mounted on mirror mount. Such that the front surface of mirror coincides with axis of rotation of rotating table (Fig.3.9-a). First of all the mirror is made perpendicular to the laser with the help of micrometer adjusting screws. Then the rotating table is rotated by an angle θ_1 equal to the angle of incidence. Then the detector is brought in the path of the laser beam reflected from the mirror surface, such that the beam hit the detector sensitive area through the apprture. The detector now is fixed in specular direction. Then a mirror is plugged into the detector aperture and the detector is adjusted till the reflected ray retraces its path (Fig.3.9-b) the rotating arm scale is then adjusted to zero and mirror is taken out of the detector aperture. And the mirror placed on the rotating table is replaced by a rough surface specimen.

3.1.7 Shape of rough surface specimens(rss): Rectangular aluminium test specimens of 30mm \times 30mm \times 10mm are made and one of their flat surface is machined giving 30mm \times 30mm of rough surface. Specimen are made on both milling and lathe machine with different cutting conditions so as to have surfaces with different roughness. On the whole fifteen specimens are made to the specifications given in table 3.2. Due to the shape of the tools used both for milling

Table 3.2
SPECIFICATION OF SPECIMENS

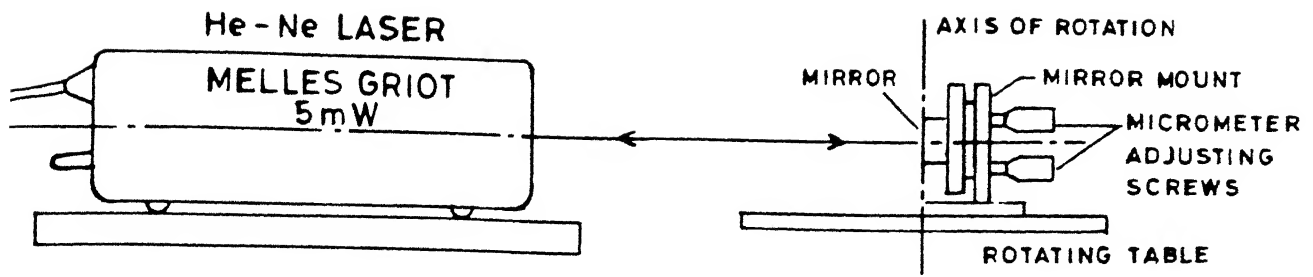
(a) FACE TURNING

imen	Feed mm/Rev	R. P. M.	Depth of Cut (mm)	R_a (Measured value) microns(μ)
	1.596	421	0.2	15.6
	0.638	421	0.2	3.8
	0.199	646	0.2	1.0
	0.049	421	0.1	0.8

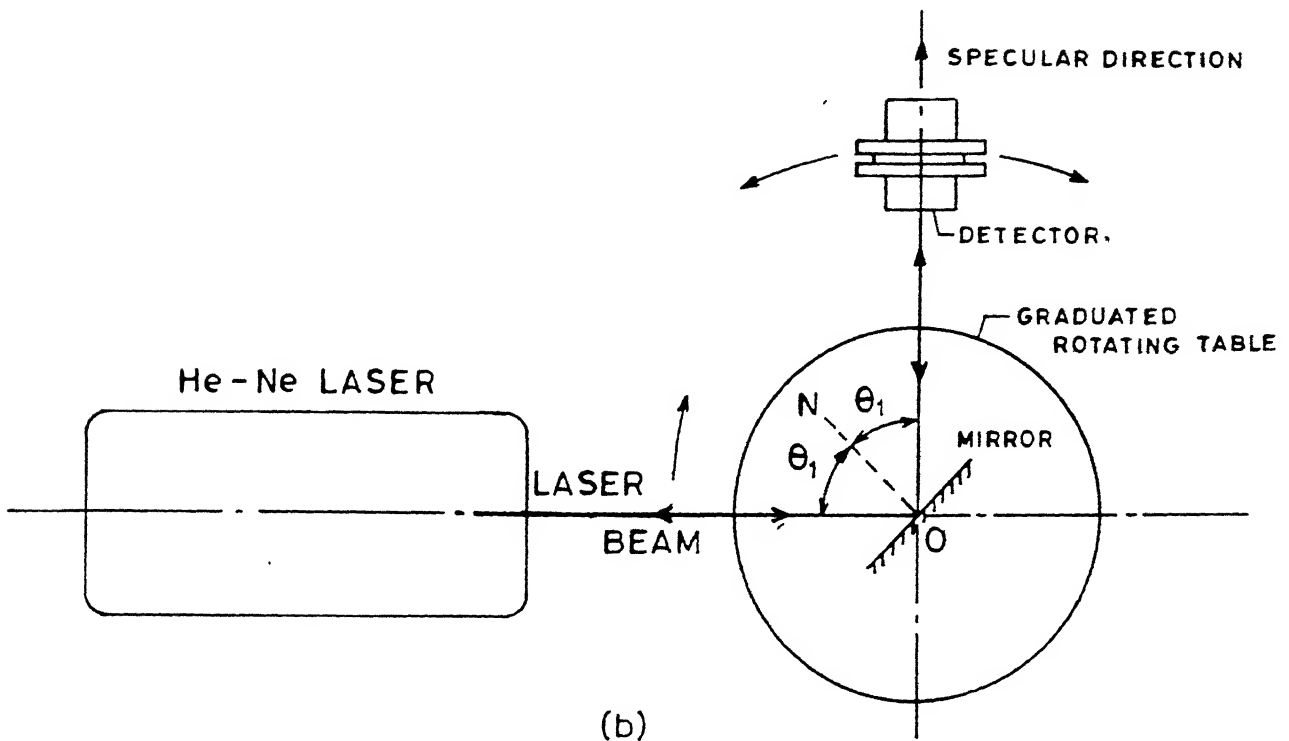
(b) FACE MILLING

imen	Feed (mm/rev)	Cutting speed (m/min)	Depth of cut (mm)	R_a	Nose radius (mm)	* Effective tool angles (Deg.)	End Cutting Edge	Side Cutting Edge
	0.01	504.5	0.2	1.5	0.25	18°	0°	0°
	0.02	504.5	0.1	1.4	0.25	18°	0°	0°
	0.06	319.6	0.1	1.5	0.25	18°	0°	0°
	0.043	504.5	0.2	1.6	0.25	18°	0°	0°
	0.045	190	0.2	0.9	1.25	22°	21.25°	0°
	0.017	504.5	0.2	0.3	1.25	22°	21.25°	0°
	0.007	781.7	0.2	0.3	1.25	22°	21.25°	0°
	0.011	781.7	0.15	0.4	1.25	22°	21.25°	0°
	0.017	319.65	0.1	0.7	1.25	2°	0°	34°
	0.01	504.5	0.2	0.4	1.25	2°	0°	34°
	0.007	781.7	0.1	0.3	1.25	2°	0°	34°

* Flytool is inclined at 39° with the vertical.



(a)



(b)

FIG. 3.9 ALIGNMENT OF DETECTOR AND LASER.

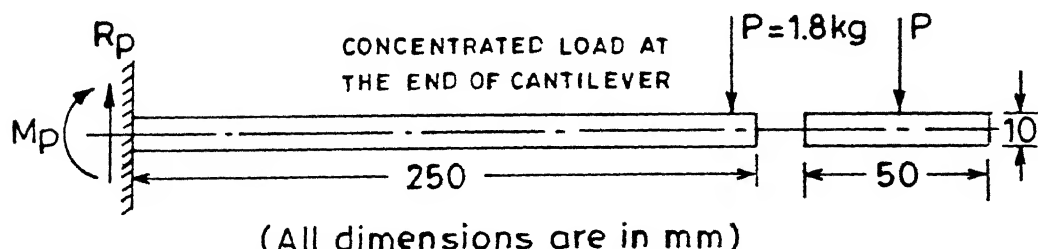


FIG. 3.10 DETECTOR ARM.

and facing (Fig.4.9-a), it is justified to assume that the undulations on the surface are triangular. Figure 4.8 shows the actual profile measured by TalySurf-10 roughness measuring instrument for some of the specimens.

3.1.8 Distance of the detector from the specimen: A compromise between the two requirements, that is, one; the point of observation should be in Fraunhofer zone and, second; that the detector should move in a radius about the point of incidence, needs to be made. Since the detector is mounted at the end of rotating arm which can be assumed as an cantilever having concentrated load at the end (Fig.3.10). Hence there is a limitation to the length of the detector arm. The calculated maximum length in our present case comes out to be 250mm.

3.2 PROCEDURE

Figure 3.1-c and Fig.3.11 shows the schematic diagram of the experimental set-up. The prepared aluminium specimens are procured from the workshop and preserved in polythene bags. The laser is inclined at 25° to the Y-axis and is at a distance of 350mm from the rough surface specimen. The spot size on the specimen is about 1.8mm in diameter. Before start of the experiment, lights are switched off and the experiment is performed in dark.

3.2.1 Angular distribution (AD) measurement: After the initial adjustment as explained in article 3.1.6, the specimen is moved till the diffraction pattern is horizontal (Fig.3.12-a) and passes

through the detector aperture. Readings are then taken at a $1/2^{\circ}$ interval both in clockwise and anticlockwise direction about the specular beam. Measured values are marked +ve which are taken away from the laser or in clockwise direction about the specular beam for the present configuration and -ve for those readings taken in anticlockwise direction, i.e. towards the laser as shown in figure 3.11. Then these measured values of voltage are plotted against $(\theta_s - \theta_i)$. Where θ_s is the scattering angle w.r.t normal. AD is measured at different angles of incidence (θ_i) and for different specimens.

3.2.2 Measurement of specular intensity: This involves changing the angle of incidence by rotating the specimen. The detector has to move twice the angle moved by specimen, to remain in specular direction. The initial adjustment is done by rotating the detector such that it directly faces the laser beam. Then the specimen is inserted in between and aligned at 90° to the laser beam. Readings are taken at 1° interval and measured values of voltage are plotted against the angle of incidence.

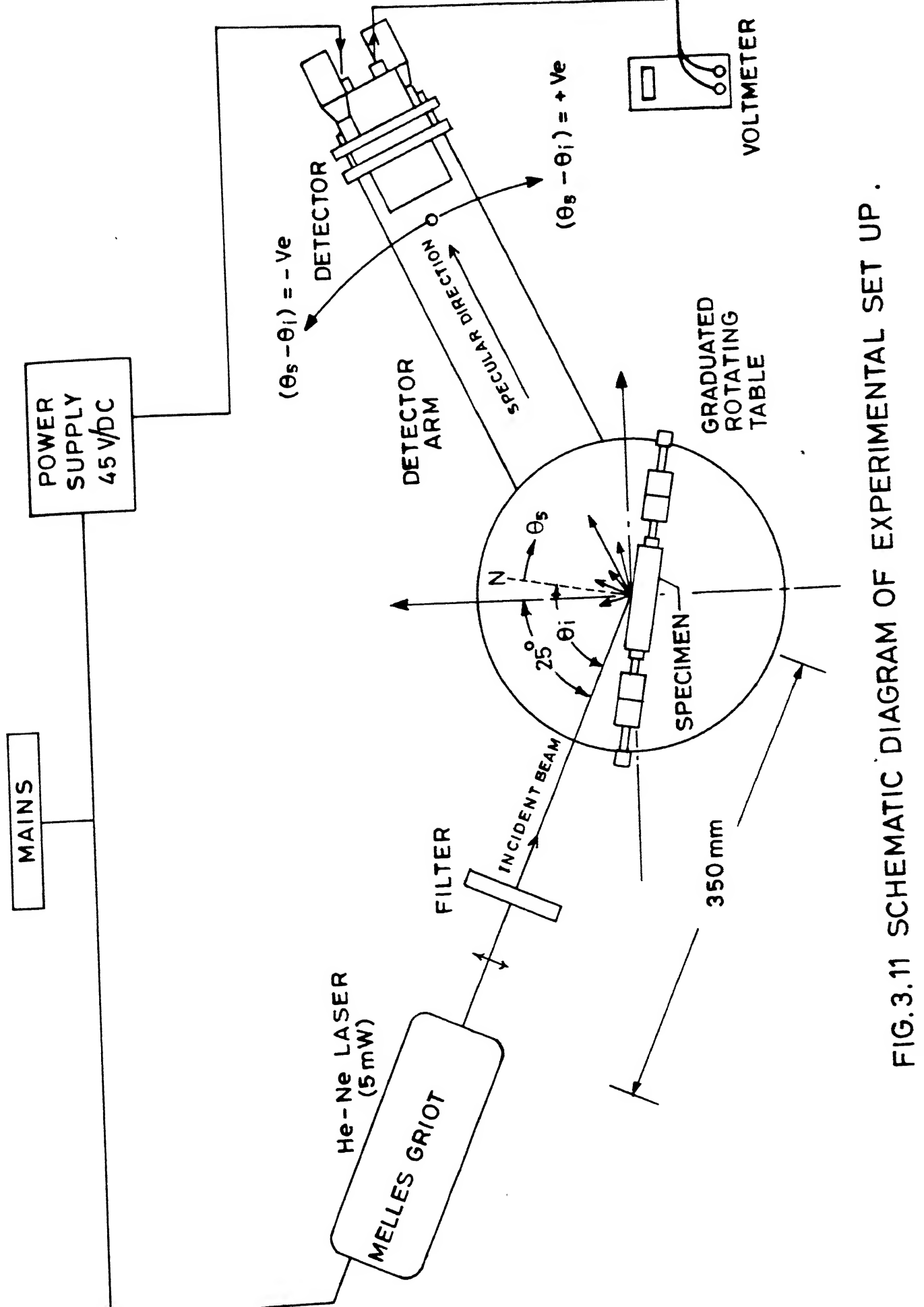
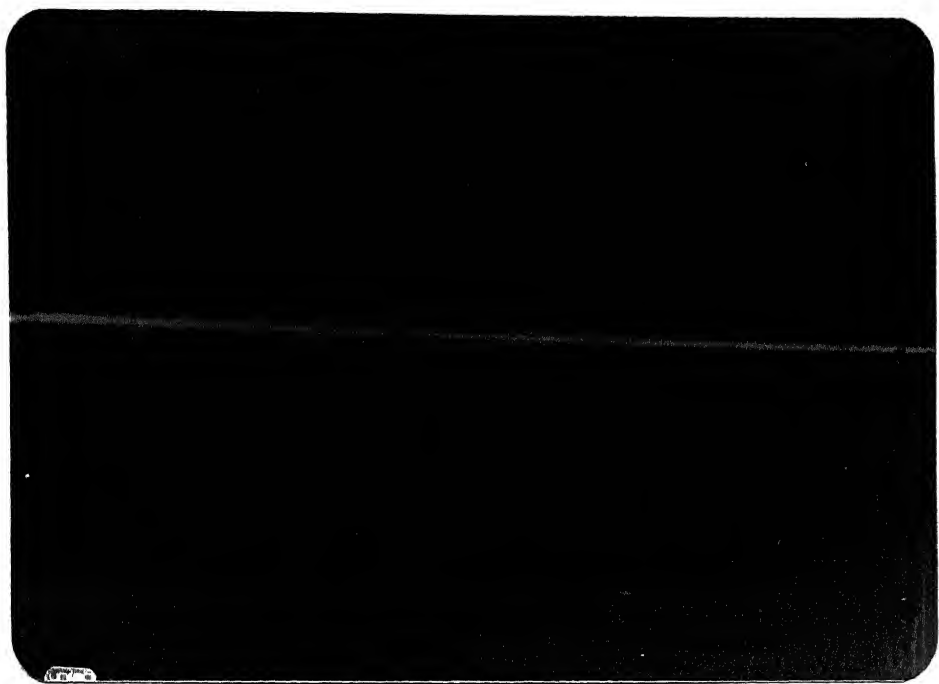
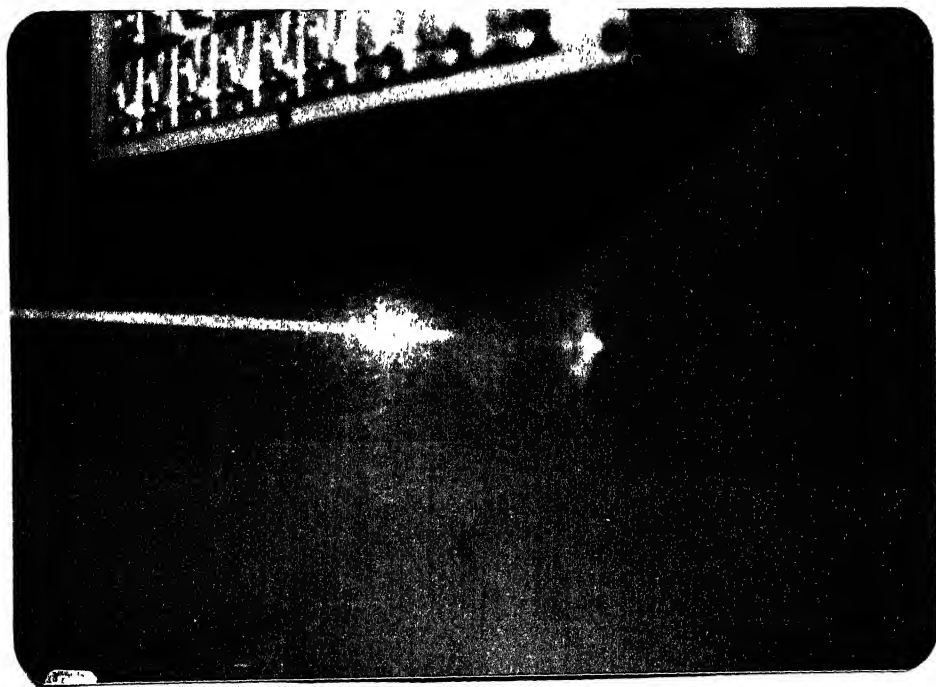


FIG. 3.11 SCHEMATIC DIAGRAM OF EXPERIMENTAL SET UP .



(a) $\theta_i = 45^\circ$



(b) $\theta_i = 87^\circ$

FIG.3.12 DIFFRACTION PATTERN AT DIFFERENT ANGLE OF INCIDENCE.

CHAPTER 4

EXPERIMENTAL RESULTS AND DISCUSSION

Angular distribution (AD) and specular intensity (I_s) is measured for incident angles of 0 to 90° by using He-Ne laser beam on specimens of aluminium machined by face turning and milling. The details of specimens and machining conditions are given in Table 3.2.

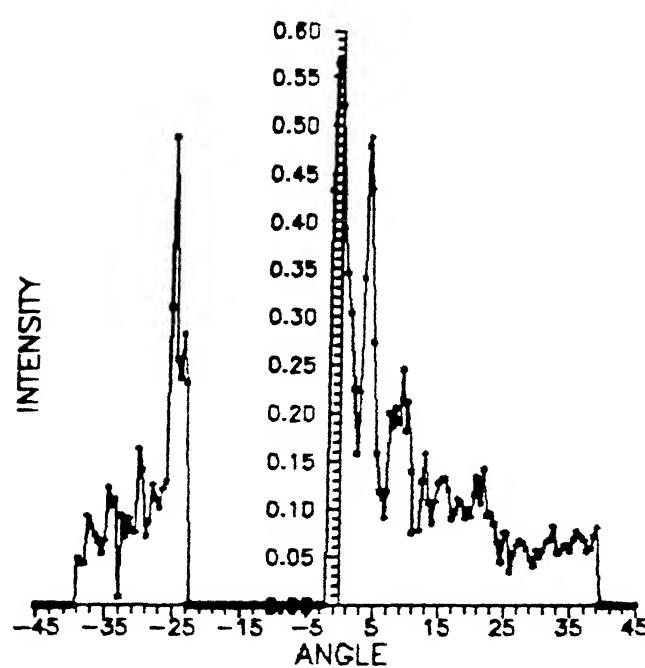
4.1 ANGULAR DISTRIBUTION

For AD measurement, the readings are taken at an interval of $1/2^\circ$ by rotating the detector while the specimen is kept fixed. Figures 4.1 to 4.4 are plots of AD obtained for face turned aluminium specimens FA-1 to FA-4 at various angles of incidence ranging from 0 to 75° . Figures 4.5 and 4.6 are plots of AD obtained for face milled aluminium specimens. MA-5 and MA-6 at various angles of incidence ranging from 0 to 87° . Table 2.1 gives the expected theoretical spacing between the modes for various specimens and calculated average spacing between the peaks (modes) for various plots, is also given in Table 2.1

4.2 SPECULAR INTENSITY

For specular intensity (I_s), the readings are taken by changing the angle of incidence by rotating the specimen at an interval of one degree as explained in article 3.2.2. Figures 4.7-a to 4.7-f are the plots of experimental and theoretical variation of I_s w.r.t angle of incidence for face milled specimens MA-5 to MA-10. The variation of angle of incidence is from 0 to 90° .

INTENSITY

(a) $\theta_i = 5^\circ$

INTENSITY

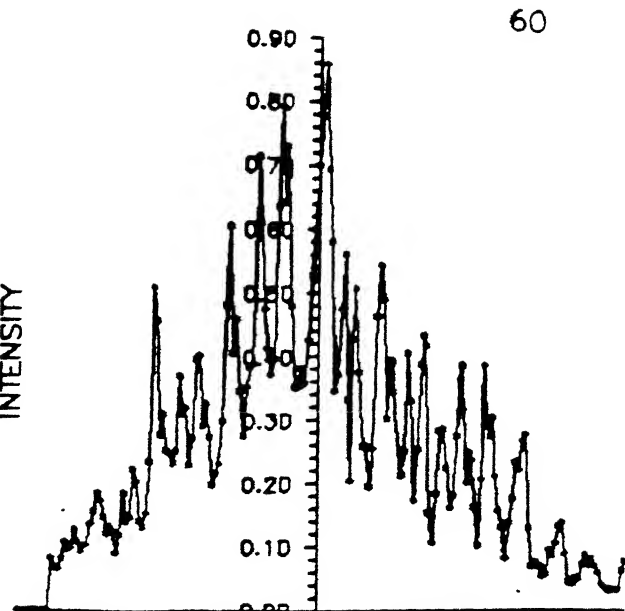
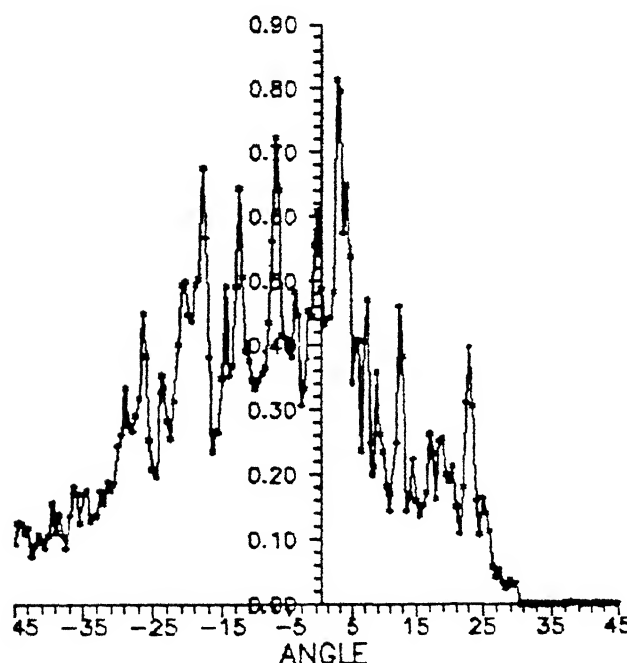
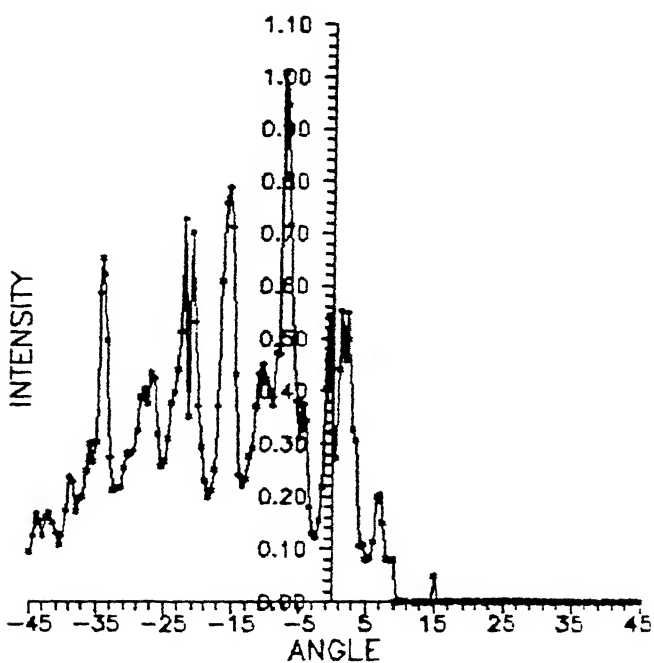
(b) $\theta_i = 25^\circ$ (c) $\theta_i = 50^\circ$ (d) $\theta_i = 75^\circ$

FIG. 4.1 AD MEASUREMENT FOR VARIOUS ANGLES OF INCIDENCE FOR SPECIMEN NO. FA-1

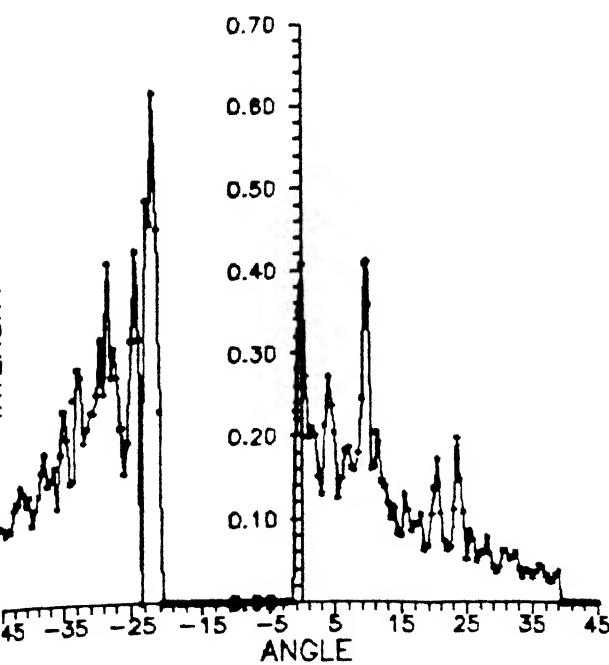
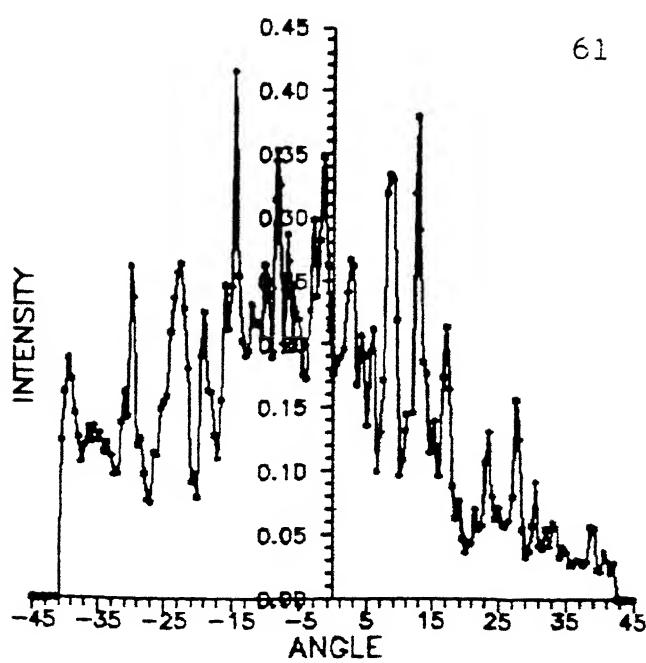
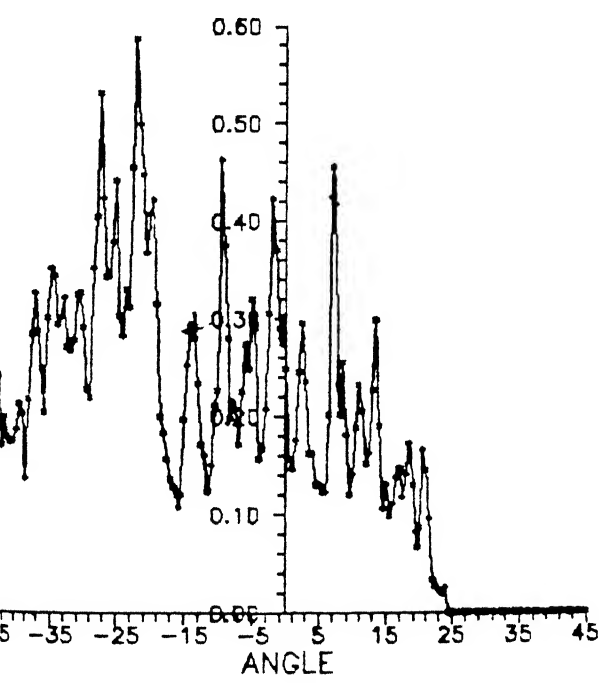
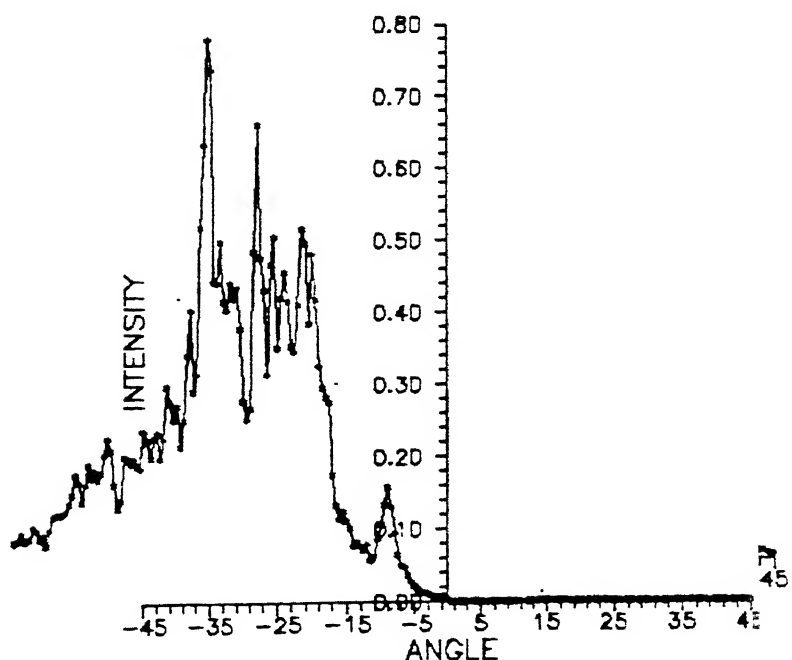
(a) $\theta_i = 5^\circ$ (b) $\theta_i = 25^\circ$ (c) $\theta_i = 50^\circ$ (d) $\theta_i = 75^\circ$

FIG. 4.2

AD MEASUREMENT FOR VARIOUS ANGLES
OF INCIDENCE FOR SPECIMEN NO. FA-2

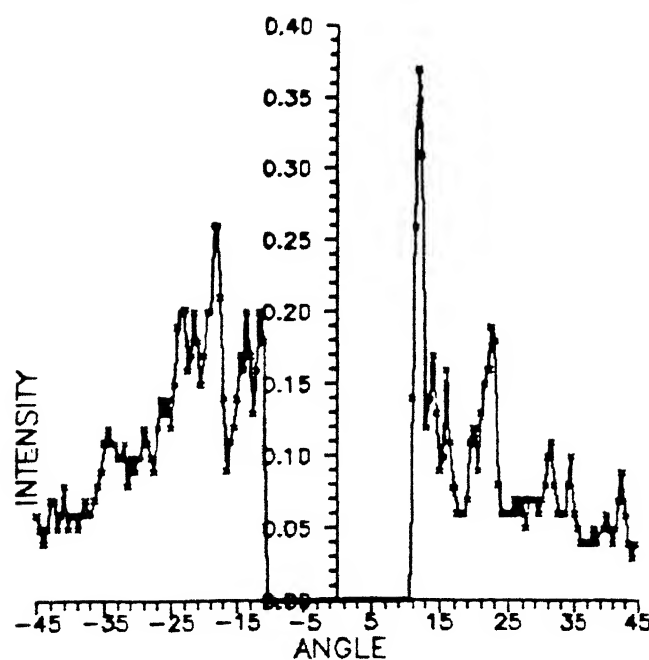
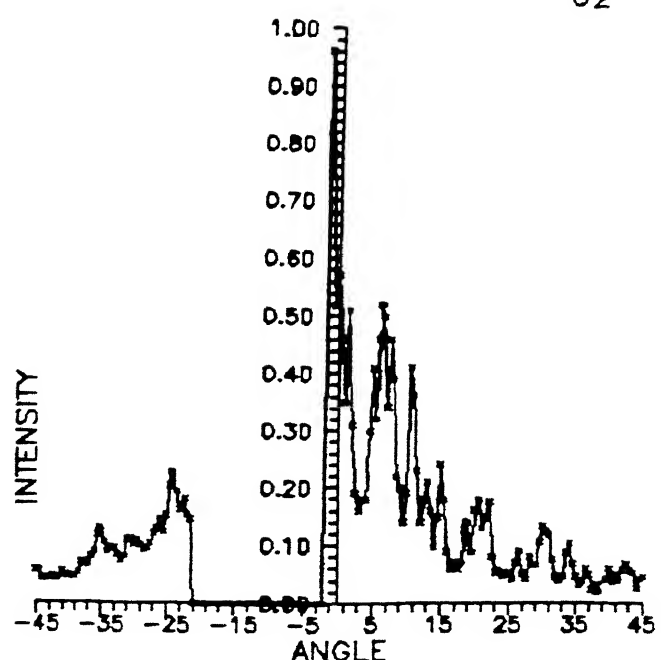
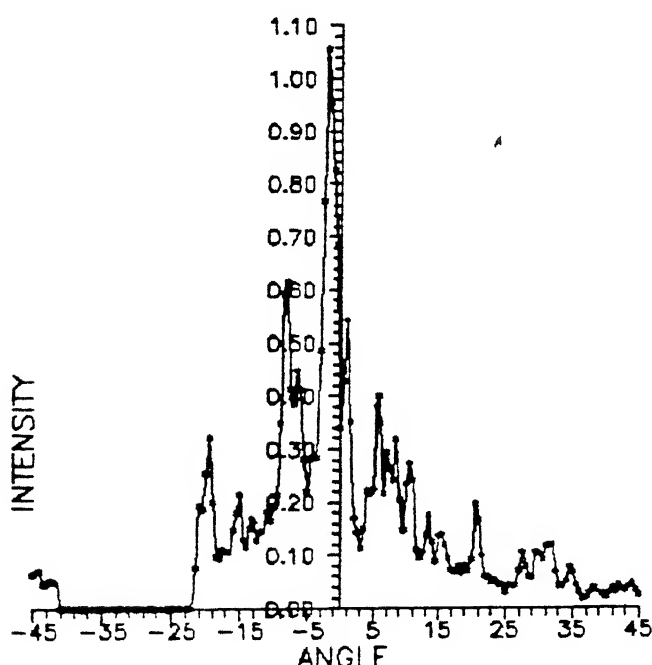
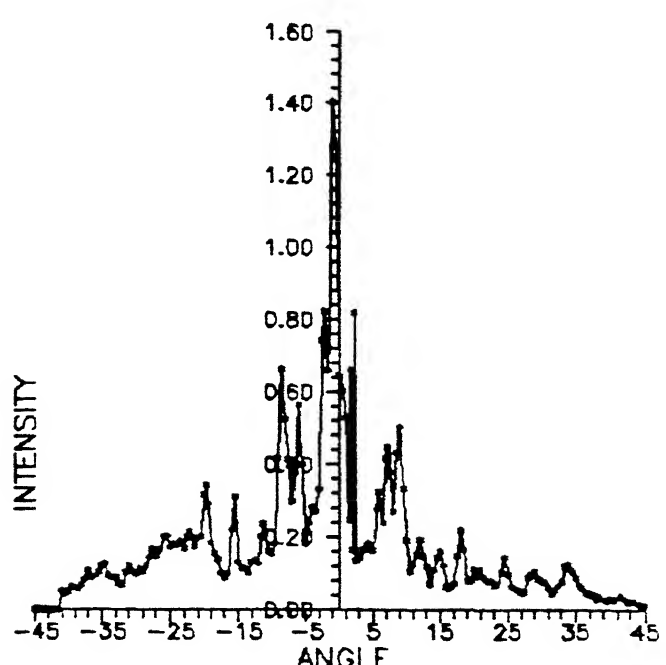
(a) $\theta_i = 0^\circ$ (b) $\theta_i = 5^\circ$ (c) $\theta_i = 30^\circ$ (d) $\theta_i = 40^\circ$

FIG. 4.3 AD MEASUREMENT FOR VARIOUS ANGLES OF INCIDENCE FOR SPECIMEN NO. FA-3

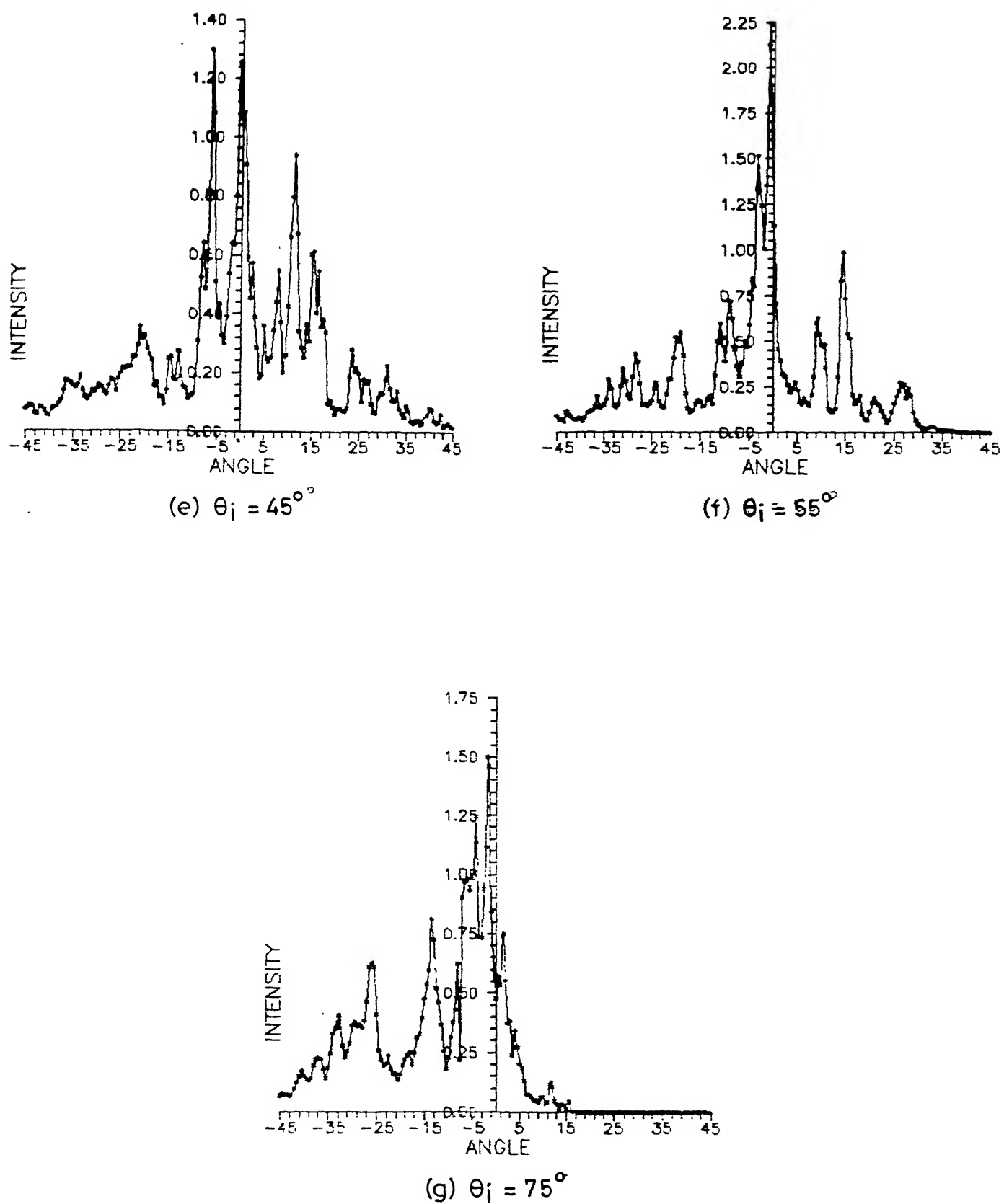


FIG. 4.3 (contd.)

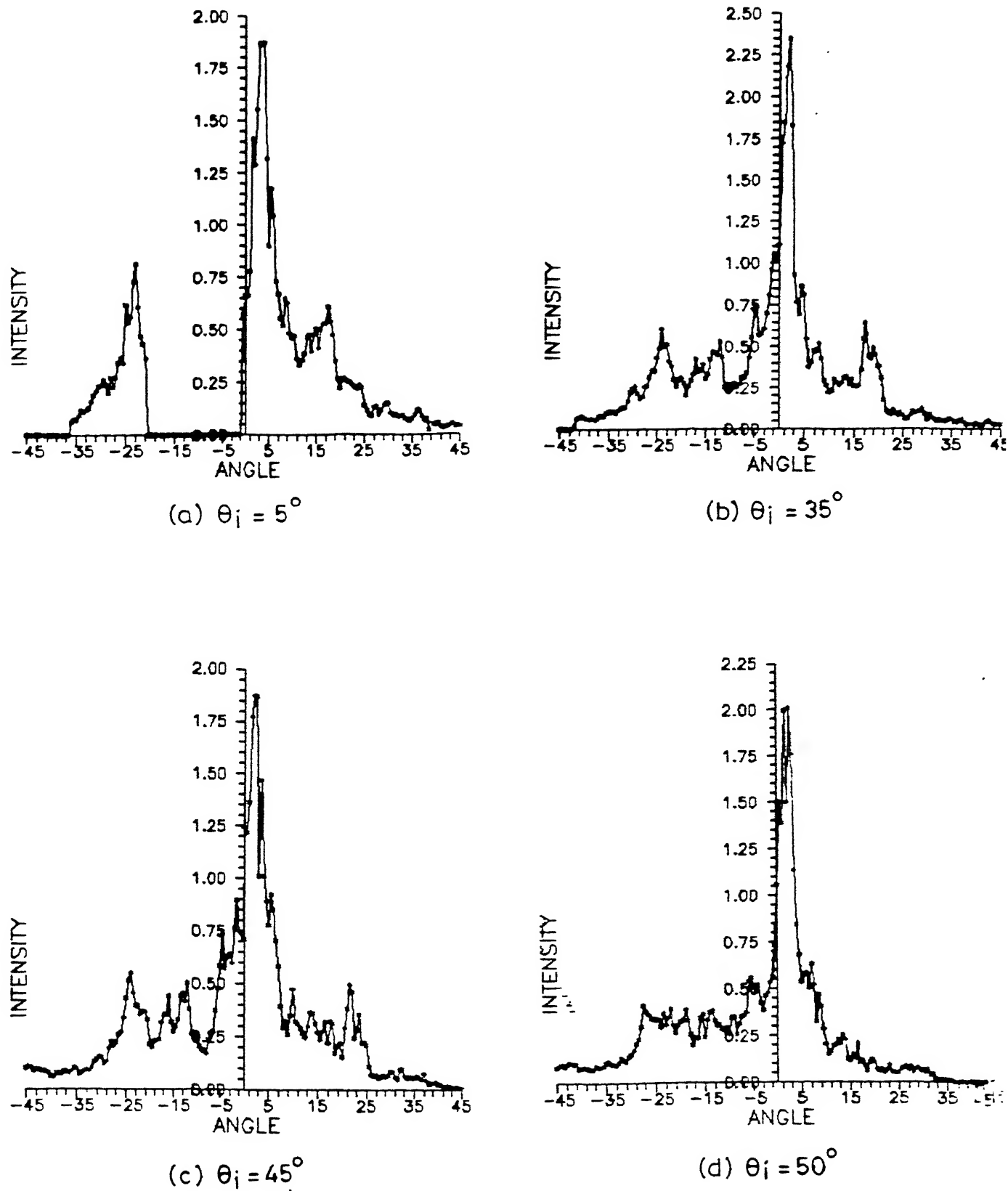


FIG. 4.4 AD MEASUREMENT FOR VARIOUS ANGLES OF INCIDENCE FOR SPECIMEN NO. FA-4

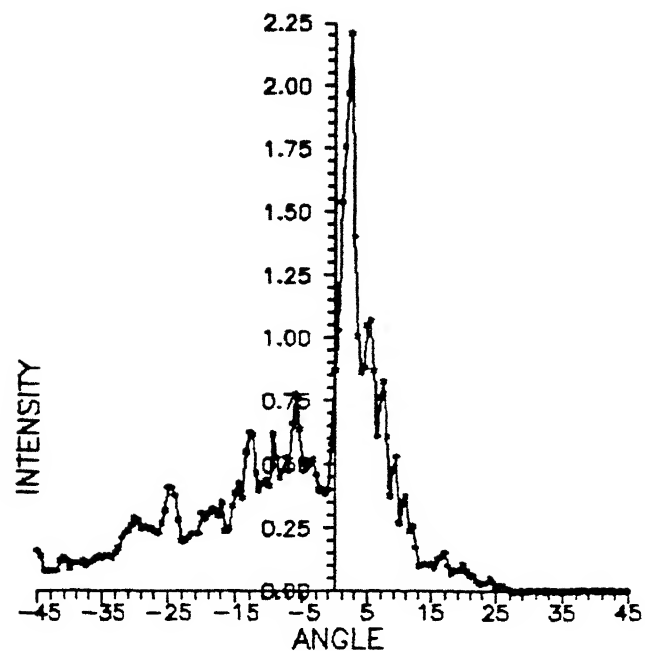
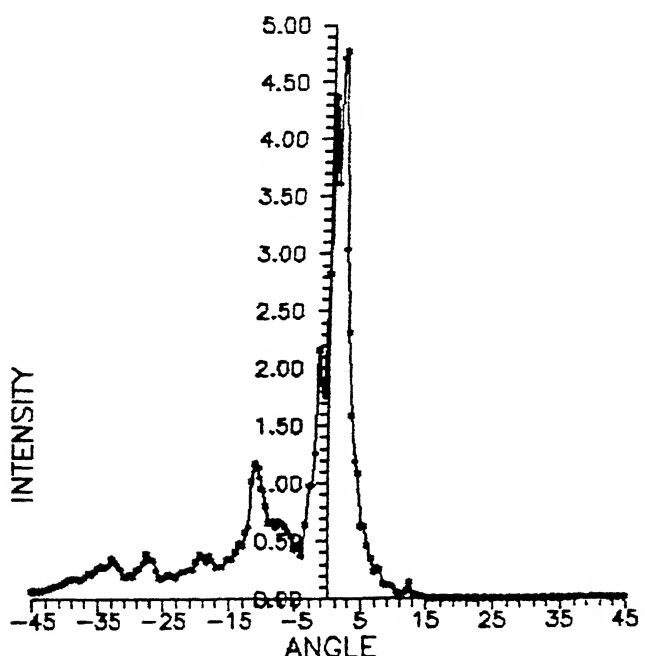
(e) $\theta_i = 60^\circ$ (f) $\theta_i = 75^\circ$

FIG. 4.4 (contd.)

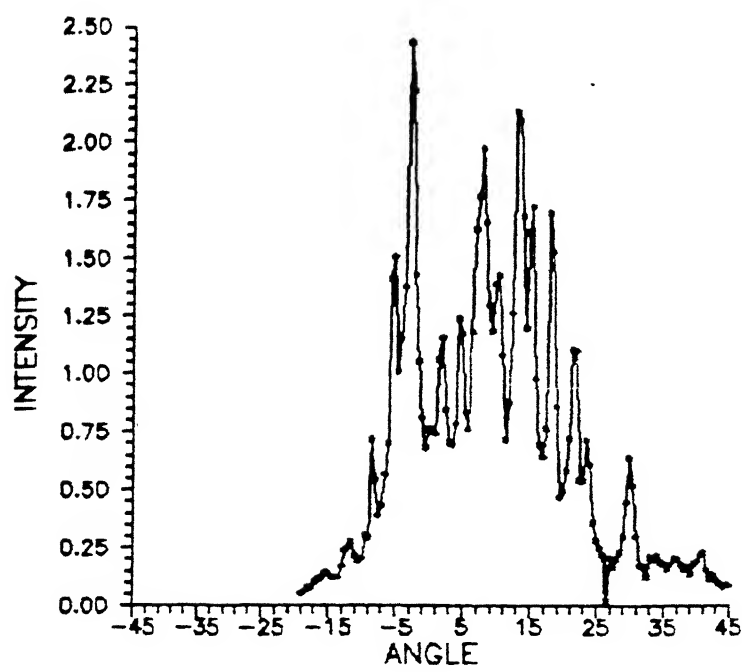
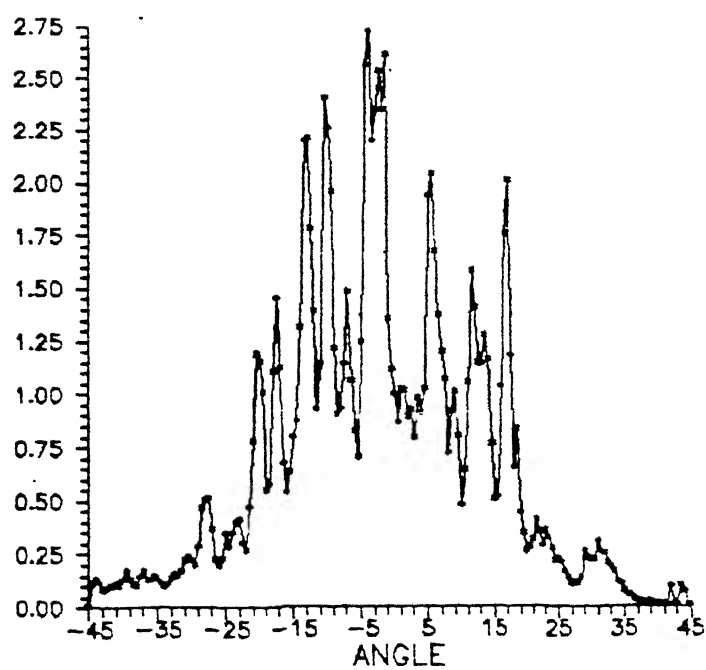
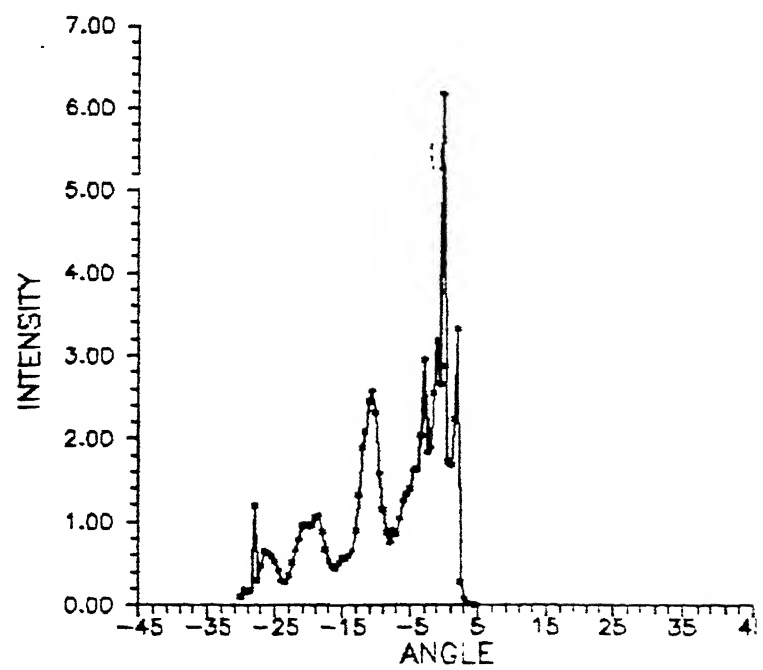
(a) $\theta_i = 10^\circ$ (b) $\theta_i = 45^\circ$ (c) $\theta_i = 86^\circ$

FIG. 4.5 AD MEASUREMENT FOR VARIOUS ANGLES
OF INCIDENCE FOR SPECIMEN NO. MA-5

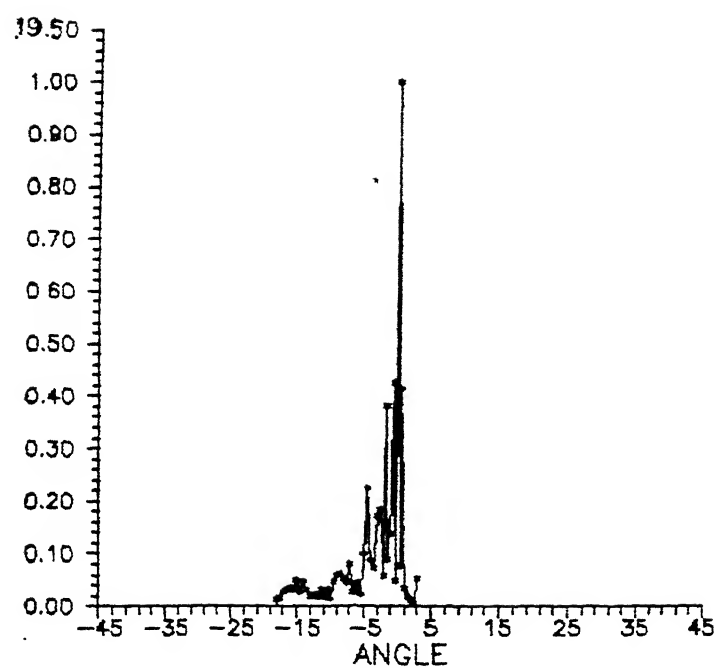


FIG. 4.6 AD MEASUREMENT FOR SPECIMEN NO. MA-6

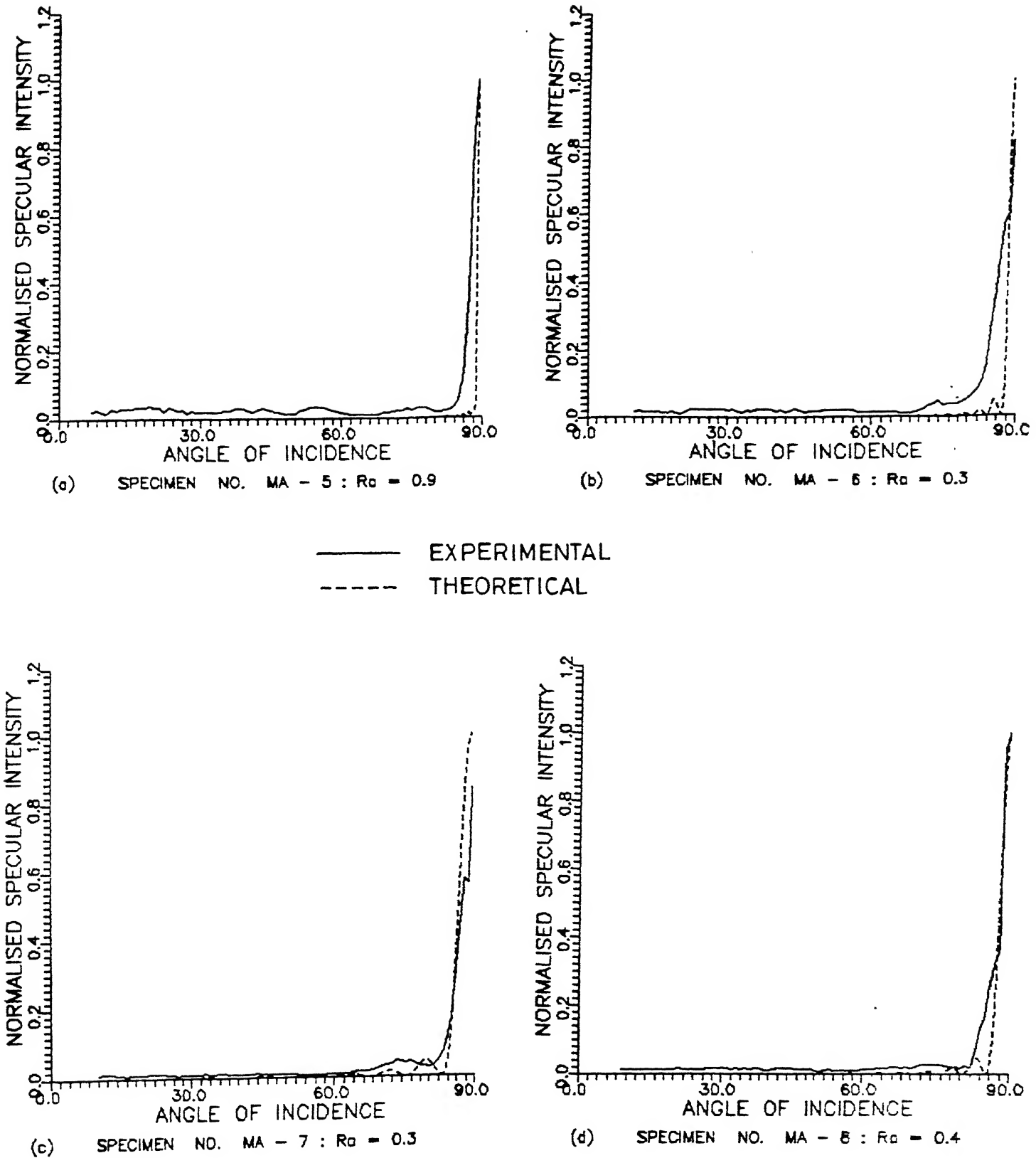


FIG. 4.7 VARIATION OF SPECULAR INTENSITY WITH INCIDENCE ANGLE.

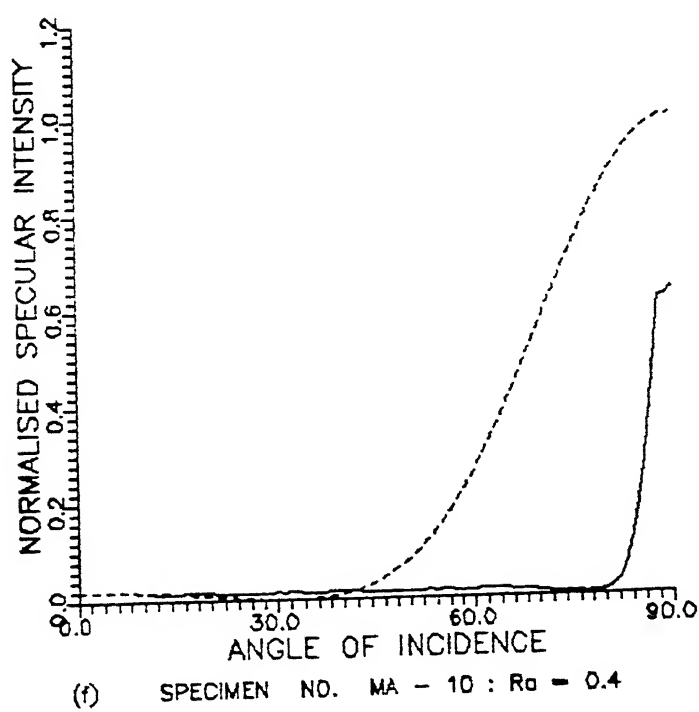
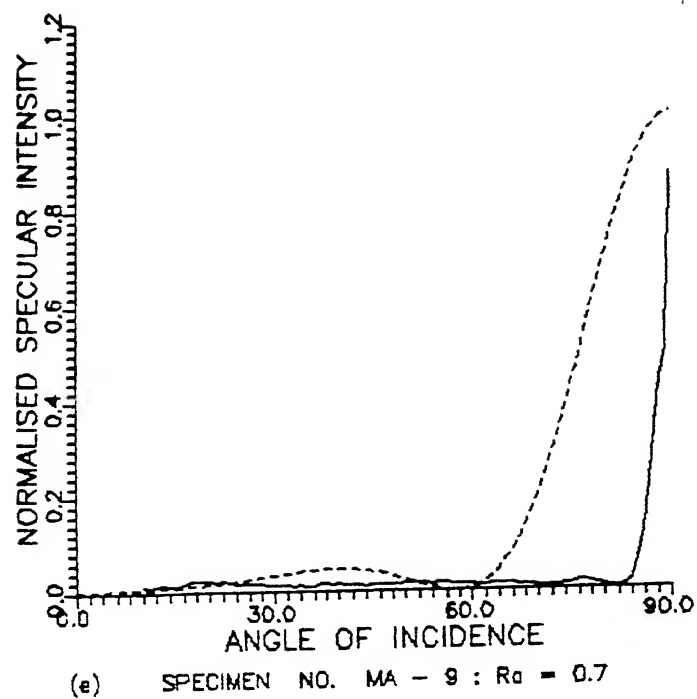


FIG. 4.7 (contd.)

4.3 ROUGHNESS PROFILE

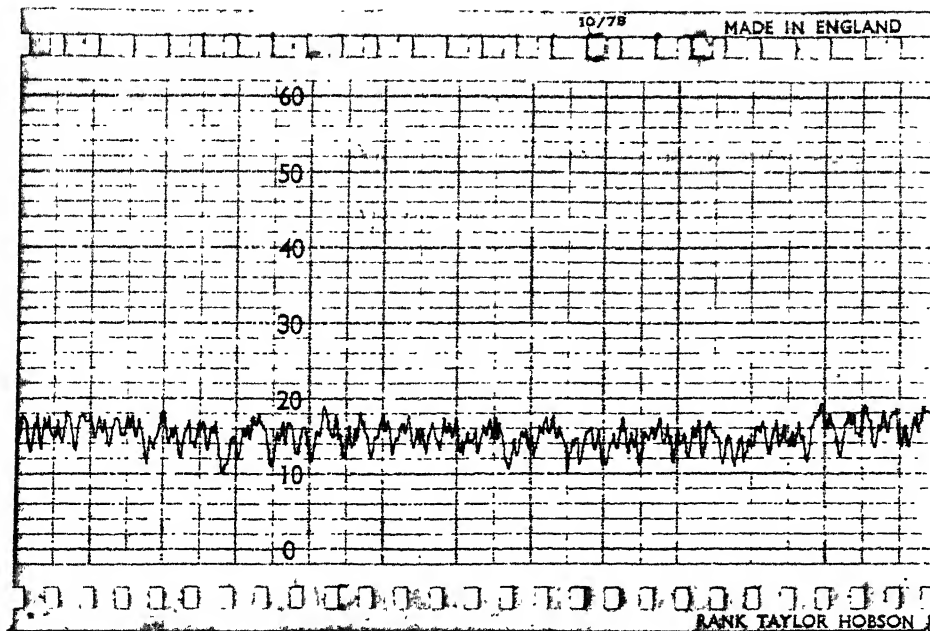
Roughness records are taken by 'Talysurf-10 Roughness Measuring Instrument'. These records are shown for specimens FA-2 and MA-2 in Figure 4.8.

4.4 DISCUSSION

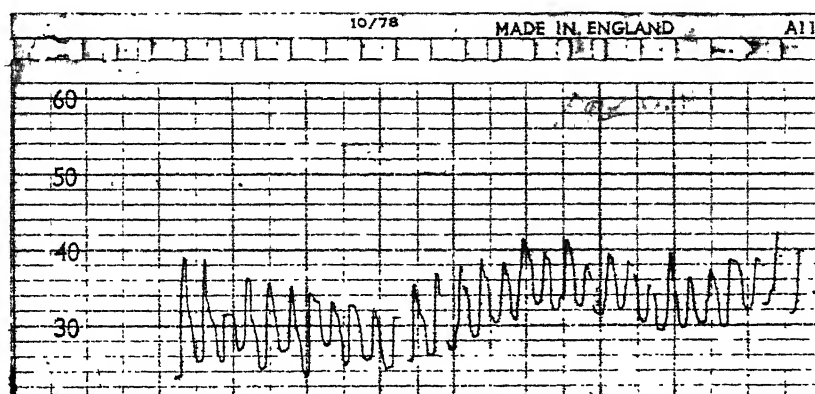
4.4.1 Angular distribution: All the AD plots show a No. of peaks. The peaks for specimen FA-1 (with higher $R_a = 15.6\mu$), are very prominent, specially for $\theta_i = 25^\circ$ and 50° (Figure 4.1) as compared to the peaks for specimen FA-3 for lower $R_a = 1.0\mu$ (Figure 4.3) and specimen FA-4, $R_a = 0.8\mu$ (Figure 4.4). For milling specimen MA-5, $R_a = 0.9\mu$, peaks are distinctly seen for lower value of angle of incidence. However peaks come closer to the specular direction for specimen MA-6, $R_a = 0.3\mu$ (Figure 4.6).

Theoretical separation of these peaks are given in Table 2.1. The average spacing of the experimental AD measurements for some of the specimens is also given. Experimental values are much higher than the theoretical spacing of peaks. This may be due to the fact that the surface profile (Figure 2.7) may not be a triangular surface with smooth reflecting surface as assumed in the theory. Furthermore due to the corner radius of the order of 0.25mm to 1.25mm, the surface profile is expected to be circular with micro-irregularities as shown in Figure 4.9, specially at low feeds and depth of cut used in the experiment. Therefore it is not possible to relate the peak spacing from AD plots to spatial wavelength and roughness of surface.

4.4.2 Specular Intensity: Plots of variation of specular intensity with angle of incidence for different specimens show that all surfaces tend to reflect most of the incident light



(a) SPECIMEN NO. MA-2



(b) SPECIMEN NO. FA-2

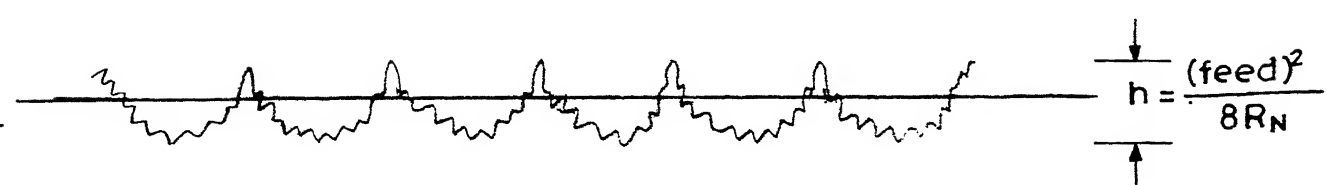
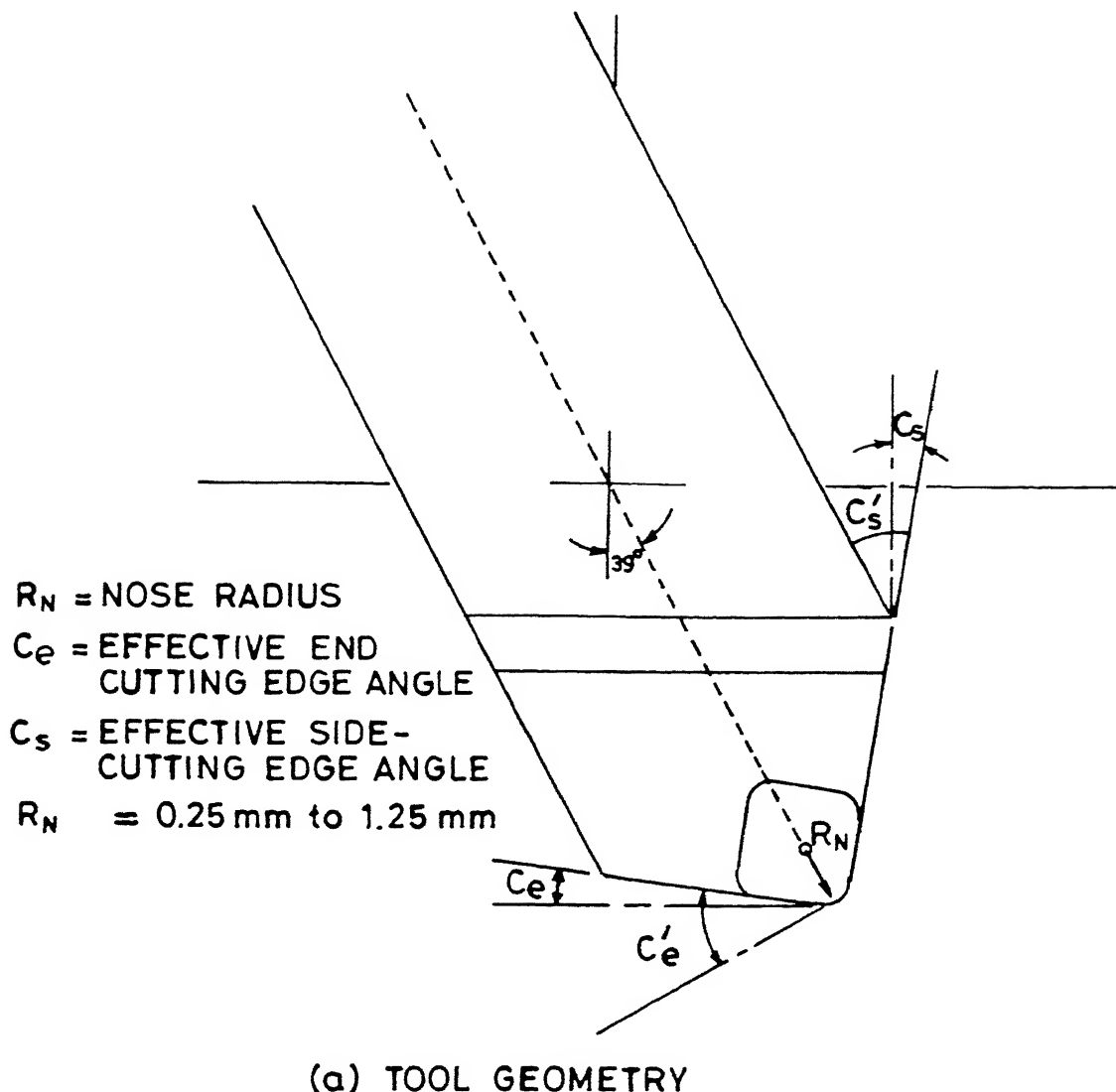
HORIZONTAL MAGNIFICATION=20
VERTICAL MAGNIFICATION=1000

FIG. 4.8 SURFACE PROFILE BY TALYSURF-10
ROUGNESS MEASURING INSTRUMENT

specularly at near grazing angles of incidence. Small amount of light is reflected in specular direction at less than 80° angle of incidence. Table 4.1 gives the theoretical and approximate experimental angle of incidence (θ_{ir}) for which the specular intensity begins to rise for different value of roughness. The lower-theoretical values of θ_{ir} for specimen no. MA-9 and MA-10, Figure 4.7-e and 4.7-f are probably due to the fact that surfaces are much smoother theoretically, with theoretical $R_a = 0.14\mu$ and 0.08μ respectively. Experimental and theoretical I_s variation for specimen MA-5 to MA-8 show a reasonable agreement. Further more for specimen MA-9 and MA-10 the theoretical curves, assuming triangular profile are away from the experimental curves. It is expected that for circular profile the theoretical curve is likely to move towards right due to the fact that the variation of I_s with θ_i follows a Bessel function (Figure 4.10).

The variation of I_s with roughness is shown in Figure 4.11 for $\theta_i = 85^{\circ}$ and $\theta_i = 87.5^{\circ}$. It is seen that the specular intensity decreases with roughness in both the cases. The decrease is much steeper for $\theta_i = 85^{\circ}$, furthermore there is a large scatter of data for $\theta_i = 87.5^{\circ}$. The intensity decreases exponentially for $\theta_i = 85^{\circ}$. The relation given in figure 4.11 can be used to relate I_s for measuring R_a ranging from 0.3 to 1.0 μm , as the intensity does not vary appreciably beyond 1.0 μm which is the order of wavelength of He-Ne laser.

The ratio R_{15} of intensity in the specular direction I_s to the intensity in the direction 15 degrees off-specular I_{15} is plotted against roughness for various values of $\theta_i (25^{\circ}, 50^{\circ}, 75^{\circ})$ in figure 4.12. In general, R_{15} show a steep fall upto $R_a = 4 \mu\text{m}$



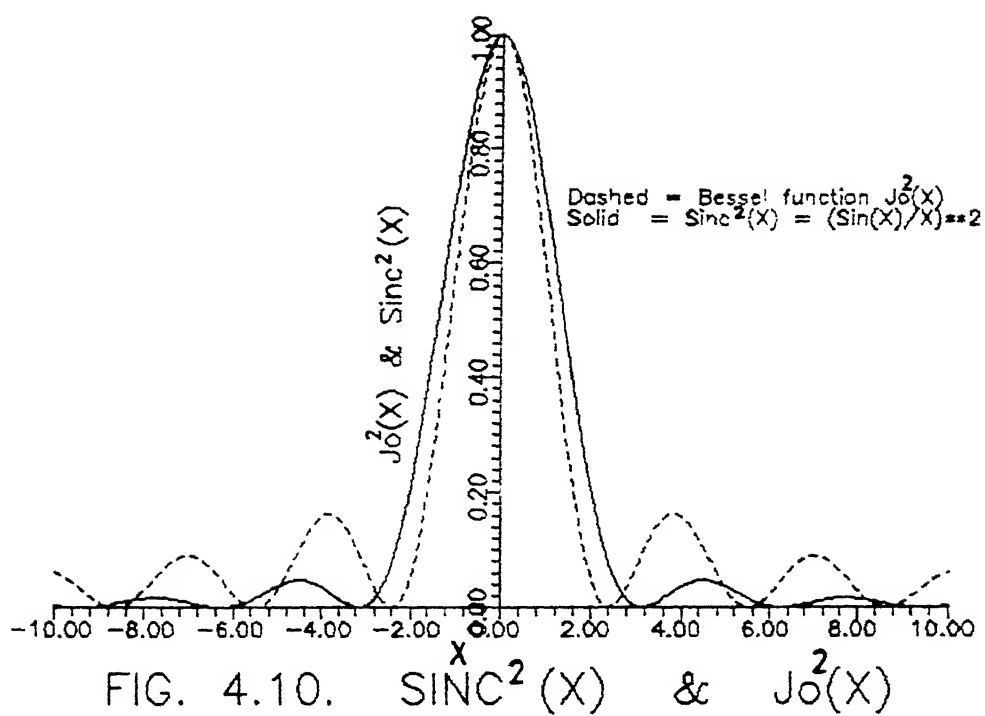
(b) CIRCULAR PROFILE WITH MICRO IRREGULARITIES

FIG. 4.9 PROFILE DUE TO FINITE TOOL RADIUS.

TABLE 4.1

ANGLE OF RISE (θ_{ir})

Specimen No.	Theoretical Roughness $R_a \mu$	Angle of Rise θ_{ir} (Degrees)	
		Theoretical	Experimental
MA-5	3.97	90°	85°
MA-6	1.49	89°	80°
MA-7	0.617	89°	80°
MA-8	0.96	89°	80°
MA-9	0.144	60°	80°
MA-10	0.08	40°	80°



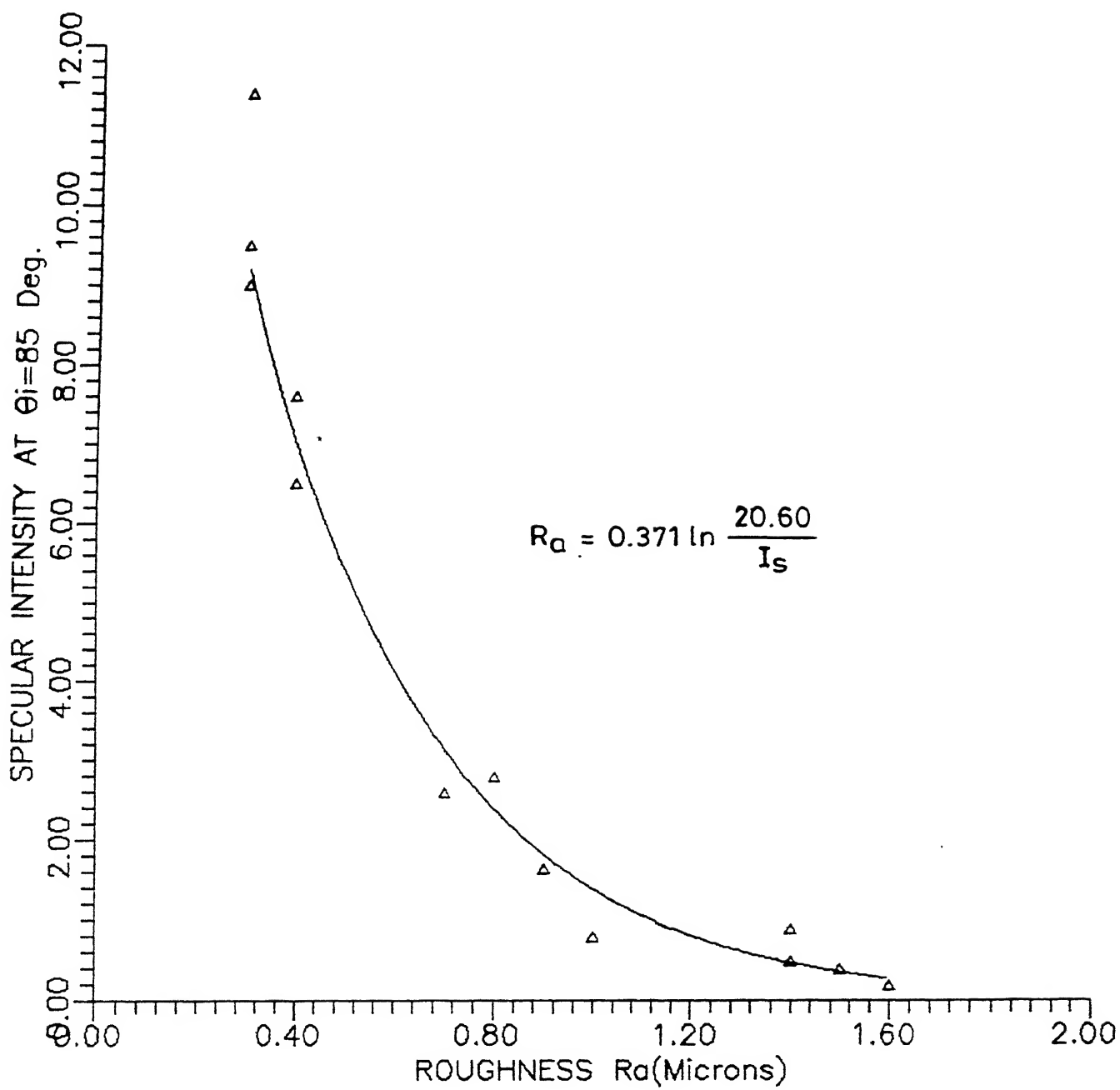


FIG. 4.11-a

VARIATION OF SPECULAR INTENSITY
WITH ROUGHNESS R_a : $\theta_i = 85^\circ$

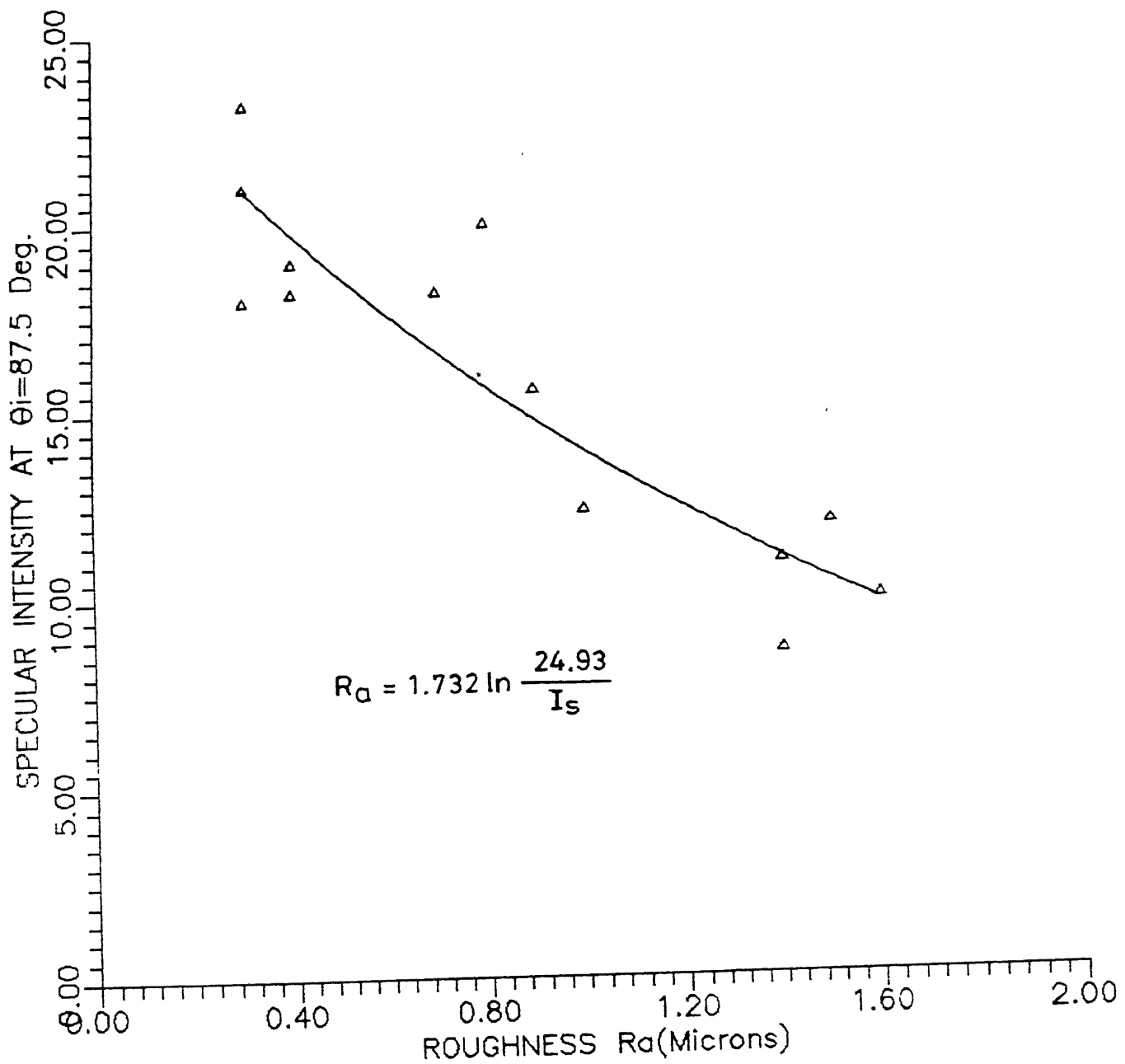


FIG. 4.11-b

VARIATION OF SPECULAR INTENSITY
WITH ROUGHNESS R_a : $\theta_i=87.5^\circ$

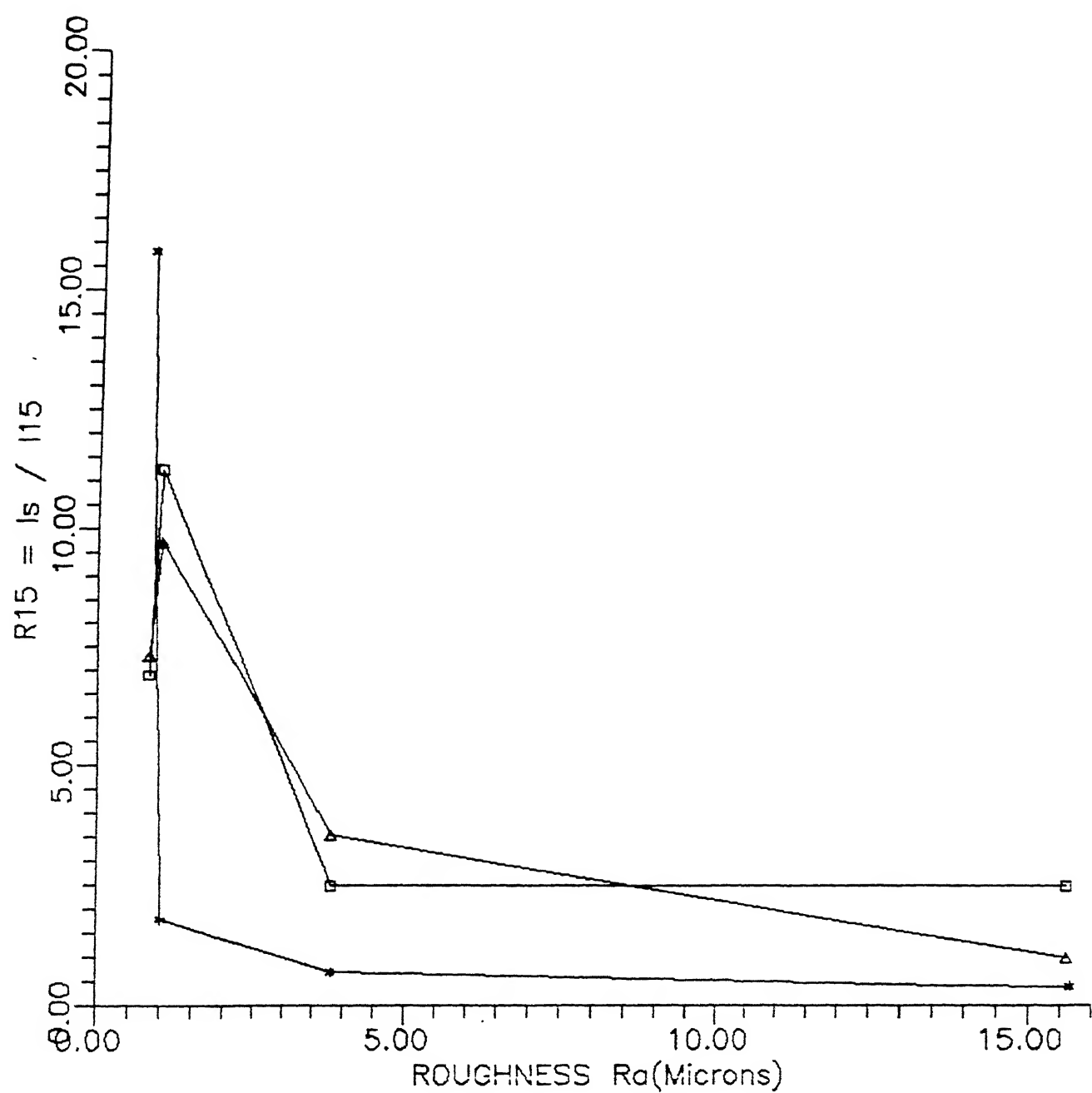


FIG. 4.12. VARIATION OF INTENSITY RATIO
 I_s/I_{15} WITH ROUGHNESS R_a

and there is a little change beyond this value. Certain research workers [9,11] have also the use of R_{30} and R_{40} for measurement of roughness R_a less than λ . However due to limited experimental results it is not possible to relate R_{15} with roughness in the present case.

CHAPTER 5

CONCLUSIONS

All the AD plots show a No. of peaks, which are very prominent for higher value of roughness. However, the average experimental spacing are much higher than the theoretical spacing of peaks. Therefore it is not possible to relate the peak spacing from AD plots to the spatial wavelength of surface.

Variation of specular intensity I_s with angle of incidence show that all surfaces tend to reflect most of the incident light specularly at near grazing angles of incidence. Experimental and theoretical I_s variation show a reasonable agreement.

The variation of I_s with roughness show that specular intensity decreases with roughness. The decrease is much steeper for $\theta_i = 85^\circ$ than for $\theta_i = 87.5^\circ$. The relation given in figure 4.11 can be used to relate I_s for measuring R_a ranging from 0.3μ to 1.0μ at near grazing angle of incidence of 85° .

The possibility of relationship between R_{15} (ratio of intensity reflected in specular direction to intensity reflected in an 15° off-specular direction) and roughness cannot be found from limited experimental results.

SUGGESTIONS FOR FURTHER WORK

In the present work, experiments are done with aluminium surface with periodic irregularities. This can be extended to other materials also. Another extension of the work can be the study of random rough surfaces using He-Ne laser. Furthermore the

scattered intensity measuring instrument can be mechanised by attaching a stepper motor to it. The detector itself can be mounted on an assembly to enable it to rotate about Y-axis for the study of scattered intensity in three dimensions.

APPENDIX

(A) BESEL FUNCTION

$$J_m(x) = \sum_{s=0}^{\infty} \frac{(-1)^s}{s!(m+s)!} (x/2)^{m+2s}$$

Where $(m+s)! = I(m+s+1) = \int_0^{\infty} e^{-t} t^{m+s} dt$

(B) SINC FUNCTION

$$\text{sinc}(x) = \frac{\sin(x)}{x}$$

(C) PROGRAMME TO CALCULATE $J_0(x)$, $\text{sinc}(x)$ and eq. No. (25)

SECTION 2.2.1b

```

c _____
c This programme is for SPECULAR direction only !
c Programme wrtn by Rajnish Kashyap under the supervision of
c Dr.G.S.Kainth(prof. Mech.) & Dr.K.K.Sharma(Head CELT ) IIT.kanpur
c ..... .
c ..... .
c _____
c implicit double precision (a-h,o-z)
c open(unit=22,file='bessel')
c open(unit=23,file='sinc')
c x=-10.0
c do 999 kk=0,200
c _____
c bessel function calculation
c _____
c rhob=1
c do 10 i=1,100
c prod1=1
c do 20 j=1,i
c d=float(j)
c b=(x/2.0)/d
c prod1=prod1*b
c continue
c prodb=prod1*(-1)**i*prod1
c rhob=rhob+prodb
c continue
c db=rhob**2
c _____
c sinc function calculation
c _____
c prods=(d*sin(x))/x
c dbs=prods**2
c write(23,11) x,dbs
c write(22,11) x,db
c x=x+.1
c format(1x,f8.3,4x,f8.5)
c continue
c stop
c end

```

c This programme calculates the theoretical intensity distribution
c due to scattering by a triangular wave. This programme is written
c by RAJNISH KASHYAP 8811606 M.Tech.LASER Technology IIT.K
c

```
implicit double precision (a-h,o-z)
common t1,rkh,sk,ratio,r11,r12,r1,r21,nen
dimension t22(10,200),ri(10,200)
open(unit=21,file='new.out')
open(unit=22,file='cash.dat1')
c.....hene=wavelength of he ne laser.....
c.....sk = propagation vector =2pi/lambda.....
r=200.0
c ... r=distance of detector from the specimen .....
rewind 22
a=3.1415925/180.0
hene=6328.193e-07
sk=2.0*3.1415925/hene
do 67 j=1,7
c.....2h= height of the triangular wave .....
r21=1.8
read(22,*,end=90)feed,rpm,phi11,phi22,t
write(21,10)feed,rpm,phi11,phi22,t
phi1=phi11*a
phi2=phi22*a
r1=feed/rpm
ratio=r1/hene
h=(r1/2.0)/((1/dtan(phi1))+(1/dtan(phi2)))
r11=2.0*h/dtan(phi1)
r12=r1-r11
rkh=sk*h
t1=t+a
nen=r21/(r1*dcos(t1))
r21=r1*f1ocat(nen)
print*, 'No. of Triangles=',nen,' Base of beam=',r21
c..... 1.8 =dia of the laser beam.....
c... at the base at the point of incidence .....
c ... . . . . . . . . . . . . . . . . . . . . .
t21=t-45.0
tt=t+45.0
if(tt.gt.90)then
mt=((90.0-t)*2.0)+(45.0*2.0)+2.0
else
mt=182
endif
do 45 m=2,mt
t22(j,m)=t21
t2=t22(j,m)*a
x=r1/2.0
mu=0
real=0
rimag=0
do 55 n=0,(nen-1)
t2x=datan(((r21/2.0)-x)/(r1*dcos(t2))+dtan(t2))
call intensity(t2x,mu,x,freal,fimag)
real=real+freal
rimag=rimag+fimag
x=x+r1
mu=mu+1
55 continue
ri(j,m)=(real**2+rimag**2)
t21=t21+0.5
45 continue
c..... subroutine for the calculation of max.value.....
.....
```

```

m=2
rmax=0
20  if(ri(j,m).gt.rmax)rmax=ri(j,m)
m=m+1
if (m.lt.mt)goto 20
write(21,*)' Rmax.=',rmax
c..... . . . . . . . . . . . . . . . . . . . . . . . . .
m=2
do 65 k=2,mt
ri(j,m)=ri(j,m)/rmax
m=m+1
65  continue
c .. . . . . . . . . . . . . . . . . . . . . . . . . . .
print*, 'rmax=',rmax
write(21,11)'rl=',rl,'h=',h,'rkh='
1 ,rkh,'n=',nen
write(21,13)(t22(j,m),ri(j,m),m=2,mt)
67  continue
stop
endfile 22
format(1h /1x,'feed=',f9.4,3x,'rpm=',f8.2,3x, 'phi1 =',
1 f6.2,3x,'phi2 =',f6.2,3x,'incidence='f7.2)
11 format(2x,5(a4,f10.4,3x))
13 format (1h /,6(2x,f6.1,2x,f10.8))
end
c..... . . Subroutine for Intensity . . . . . . . . . . . .
c. . . . . . . . . . . . . . . . . . . . . . . . . . . . .
subroutine intensity(t2x,mu,x,freal,fimag)
implicit double precision (a-h,o-z)
common t1,rkh,sk,ratio,r11,r12,rl,r21,nen
c . . . . . Calculation of factor F. . . . . . . . . . . .
c. F=F2((1,02):page 25 eq.45 of the book.. . . . . . .
t2x=(t2x/3.1415925)*180.0
f=((1+dcos(t1+t2x))/((dcos(t1)+dcos(t2x))*dcos(t1)))
c. p=p of the book , p no 38 eq.13. . . . . . . . . . .
p=ratio*(dsin(t1)-dsin(t2x))
c. Vx=vx of the book,p no 48.eq.no. (4). . . . . . .
vx=ek*(dsin(t1)-dsin(t2x))
c. . . . . x1=Vz h of the book,p no.48:eq.no.7. . . . . .
x1=-rkh*(dcos(t1)+dcos(t2x))
phi=2.0*3.1415925*p*float(mu)
c. . . . . phi = express: on p.no. 39,eq.(14)= e(i*2p*Pi*mu). . . .
c1=vx+(2.0*x1/r11)
c2=vx-(2.0*x1/r12)
phi1=c1*r11/2.0
phi2=(2.0*x1*r1/r12)+(c2+r11)+(c2*r12/2.0)
r1=(2.0/c1)*dsin(c1*r11/2.0)
r2=(2.0/c2)*dsin(c2*r12/2.0)
rx=r1*dcos(phi1)+(r2*dcos(phi2))
ry=(r1*dsin(phi1))+(r2*dsin(phi2))
rmag=dsqr((rx**2+ry**2)/rl)
rphase=datan(ry/rx)
tphase=rphase+phi
c. . . . . fr=intensity product. . . . . . . . . . . . .
fr=rmag*f/float(nen)
freal=fr*dcos(tphase)
fimag=fr*dsin(tphase)
return
end

```

REFERENCES

- [1] Thomas, T.R., *Rough surfaces*, Longman Inc., 1982, New York.
- [2] Takeyama, H., Sekiguchi, H., Murata, R., "IN-Process Detection of Surface in Machinery," *CIRP Annals*, vol.25, 1976, pp. 467-475.
- [3] Tanner, L.H. Fahovm, M., "A Study of the Surface Parameters of Ground and Lapped Metal Surfaces, Using Specular and Diffuse Reflection of Laser Light," *Wear*, vol.36, 1976, pp. 299-316.
- [4] Vorburger, T.V., Teague, E.C., "Optical Techniques for On-Line Measurement of Surface Topography", *Precision Engineering*, vol. , 1981, pp. 61-84.
- [5] Peters, J., Vanherck, P., Sastrodinolo, M., "Assessment of Surface Topology Analysis Techniques, " *Annals of CIRP*, vol.28/2/1979, pp. 539-554.
- [6] Beckmann, P., Spizzichino, A., *The Scattering of Electromagnetic Waves from Rough Surfaces*, Pergamon, New York, 1963.
- [7] Bennet, H.E., "Specular Reflectance of Aluminized Ground Glass and the Height Distribution of Surface Irregularities," *J. Opt. Soc. Am*, vol.53, 1963.
- [8] Tanner, L.H., "A Comparison of Talysurf 10 and Optical Measurements of Roughness and Surface Slope," *Wear*, vol.57, 1979.
- [9] Clarke, G.M., Thomas, T.R., "Roughness Measurement with Laser Scanning Analyser," *Wear*, vol.57, 1979.
- [10] Church, E.L., "The Measurement of Surface Texture and Topography by Differential Light Scattering," *Wear*, vol.57, 1979, pp. 93-105.
- [11] Church, E.L., Jenkinson, H.A., Zavada, J.M., "Measurement of the Finish of Diamond-Turned Metal Surfaces by Differential Light Scattering," *Optical Engineering*, vol.16, No.4, 1977, pp. 360-374.
- [12] Elson, J.M., Bennet, J.M., "Relation Between the Angular Dependence of Scattering and Statistical Properties Surfaces," *J. Opt. Soc. Am*, vol.69, No.1, 1979, pp. 31-47.
- [13] Church, E.L. Jenkinson, H.A., Zavada, J.M.,

"Relationship Between Surface Scattering and Microtopographic Features," Optical Engineering, vol.18, No.2, 1979, pp. 125-136.

- [14] Roger, G., Manley, K., Cheryl, L., "Characterising Gastrolith Surface Roughness with Light Scattering," Op. Comm., vol.74, No.5, 1990, pp. 279-283.
- [15] Herbert, P., Numan, M., Vagszegi, Z., "Laser Optical Roughness Measurement, IMEKO Symposium on Laser Application in Precision Measurement," Budapest, 1986.
- [16] Whitley, J.L., Kusy, R.P., Mayhow, M.J., Ruckthal, J.E., Surface Roughness of Stainless Steel and Electroformed Nickel Standards Using a He-Ne Laser," Optics and Laser Technology, vol.19, No.4, 1987, pp. 189-196.
- [17] Landing, L., Adin Mann, J., Edwards, R.V., "Analysis of a Surface Scattering Spectrometer," Journal of Opt. Soc. Am., vol.16, No.11, 1989, pp. 1692-1701.
- [18] Shiraishi, M., Sato, S., "Dimensional and Surface Roughness Controls in a Turning Operation," ASME Journal of Engineering for Industry, vol.112, 1990, pp. 79-83.
- [19] Yoo, S.M., Dornfeld, D.A., Lemaster, R.L., "Analysis and Modelling of Laser Measurement System Performance for Wood Surface," ASME Journal of Engineering for Industry, vol.112, 1990, pp. 66-112.
- [20] Young, D., Vorburger, J., Teague, C., "In-Process and On-Line Measurement of Surface Finish", Annals of CIRP, vol.29/1/1980, pp. 435-440.
- [21] Shiraishi, M., "In-Process Measurement of Surface Roughness in Turning by Laser Beams, "ASME Journal of Engineering for Industry, Jan. 1981, pp. 1-7.
- [22] Elson, J.M., Bennet, J.M., "Relation Between the Angular Dependence of Scattering and the Statistical Properties of Optical Surfaces.
- [23] Thwaite, E.G., "Power Spectra of Rough Surfaces obtained by Optical Fourier Transformation.
- [24] Stover, J.C., "Roughness characterization of Smooth Machined Surfaces by Light Scattering," Appl. Opt., vol.14, 1975.
- [25] Whitehouse, D.J., "Comparison Between Stylus and Optical Methods for Measuring Surfaces," Annals of CIRP, vol.37/20/1988, pp. 649-653.

- [26] Gaskill, J.D., *Linear Systems and Fourier Transforms, and Optics*, John Wiley & Sons, New York, 1978.
- [27] Grewal, B.S., *Higher Engineering Mathematics*, Khanna Publishers, New Delhi, 1987.
- [28] Gradshteyn, I.S., Ryzhik, I.M., *Table of Integrals, Series, and Products*, Academic Press, 1980.
- [29] Pandey, P.C., Shan, H.S., *Modern Machining Processes*, Tata McGraw-Hill, New Delhi, 1980.
- [30] Schaum's outline series on ,*Machine Design*, McGraw-Hill, Singapore, 1983.
- [31] Broadmann, R., Optische Werke, G., Thurn, G., "An Optical Instrument for Measuring the Surface Roughness in Production Control," *Annals of CIRP*, vol. 33/1/1984, pp. 403-406.
- [32] Koning, J., Schellekens, P.H.J., McKeown, P.A., "Wavelength Stability of He-Ne Lasers Used in Interferometry: Limitations and Traceability," *Annals of CIRP*, vol. 28/1/1979, pp. 307-310.
- [33] Johnston, G., Manley, Kim., Lemanski, L., "Characterizing Gastrolith Surface Roughness with Light Scattering," *Optics Communication*, vol. 74, No. 5, 1990, pp. 279-283.